

Process-based climate model development harnessing machine learning: I. a calibration tool for parameterization improvement

Fleur Couvreur¹, Frédéric Hourdin², Danny Williamson³, Romain Roehrig⁴, Victoria Volodina⁵, Najda Villefranque⁶, Catherine Rio⁷, Olivier Audouin⁸, James Salter³, eric bazile⁹, Florent Brient¹⁰, Florence Favot¹, Rachel Honnert¹¹, Marie-Pierre Lefebvre¹, Jean-Baptiste Madeleine¹², Quentin Rodier¹, and Wenzhe Xu³

¹Université Toulouse, CNRM, Météo-France, CNRS

²LMD

³University of Exeter

⁴CNRM, Université de Toulouse, Météo-France, CNRS

⁵The Alan Turing Institute

⁶Centre National de Recherches Météorologiques

⁷Centre national des recherches météorologiques (CNRM), Université de Toulouse, Météo-France, CNRS

⁸CNRM, ⁹ University of Toulouse, Météo-France, CNRS

⁹Météo-France/CNRS

¹⁰CNRM/CNRS/Météo-France

¹¹Météo-France, CNRM-CNRS UMR-3589

¹²Laboratoire de Météorologie Dynamique

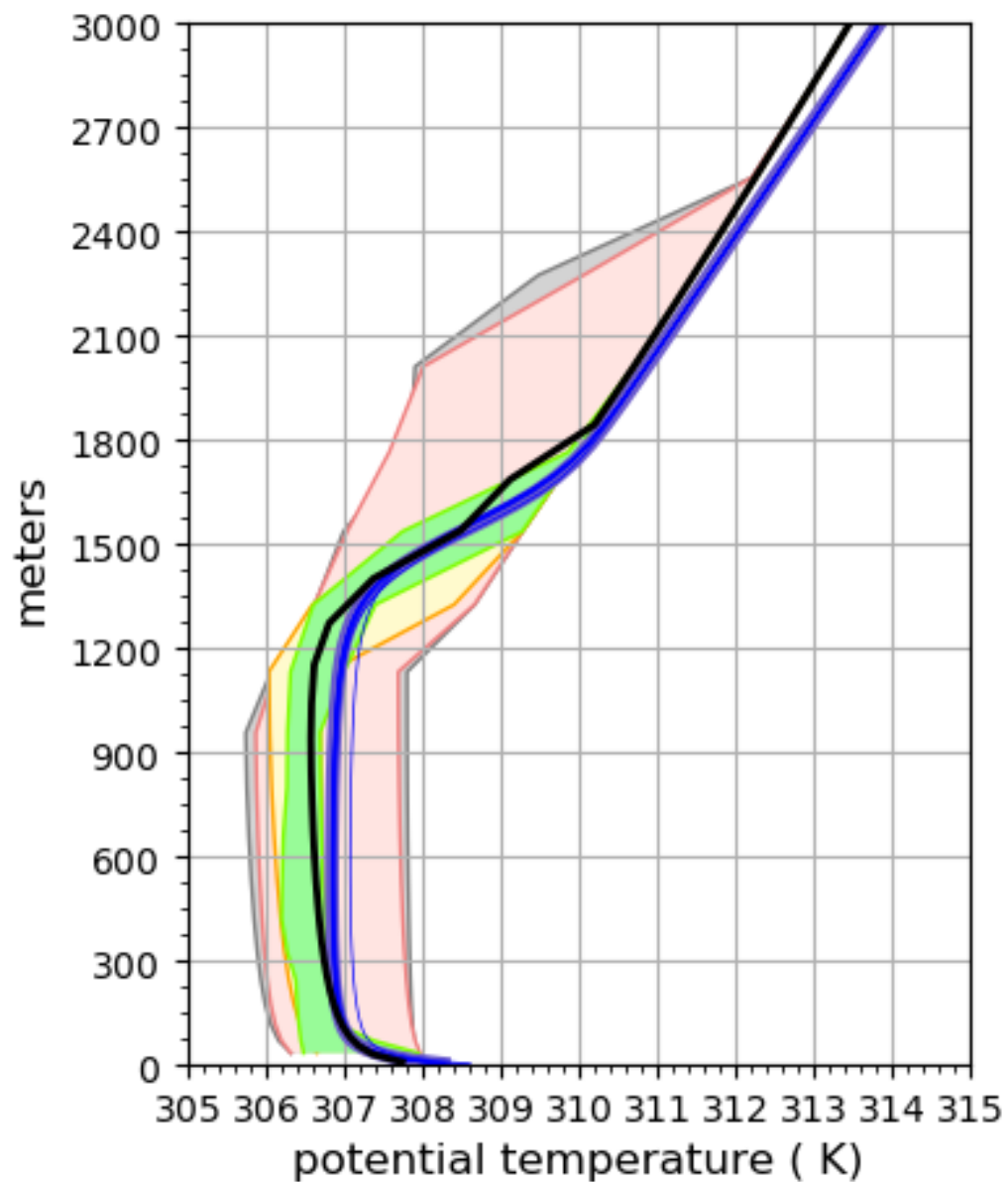
November 22, 2022

Abstract

The development of parameterizations is a major task in the development of weather and climate models. Model improvement has been slow in the past decades, due to the difficulty of encompassing key physical processes into parameterizations, but also of calibrating or tuning the many free parameters involved in their formulation. Machine learning techniques have been recently used for speeding up the development process. While some studies propose to replace parameterizations by data-driven neural networks, we rather advocate that keeping physical parameterizations is key for the reliability of climate projections. In this paper we propose to harness machine learning to improve physical parameterizations. In particular we use Gaussian process-based methods from uncertainty quantification to calibrate the model free parameters at a process level. To achieve this, we focus on the comparison of single-column simulations and reference large-eddy simulations over multiple boundary-layer cases. Our method returns all values of the free parameters consistent with the references and any structural uncertainties, allowing a reduced domain of acceptable values to be considered when tuning the 3D global model. This tool allows to disentangle deficiencies due to poor parameter calibration from intrinsic limits rooted in the parameterization formulations. This paper describes the tool and the philosophy of tuning in single-column mode. Part 2 shows how the results from our process-based tuning can help in the 3D global model tuning.

Figure 4.

2009-12-11 15:30



2009-12-11 15:30

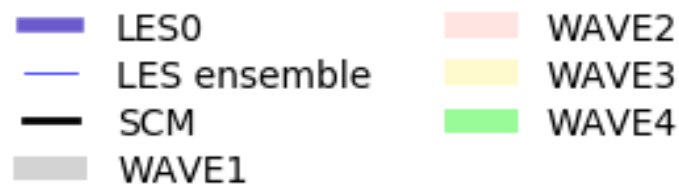
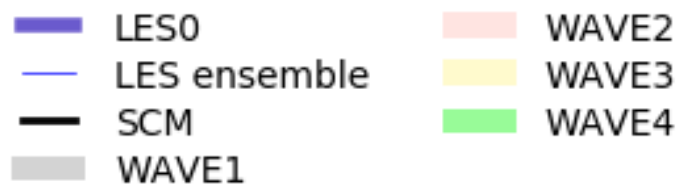
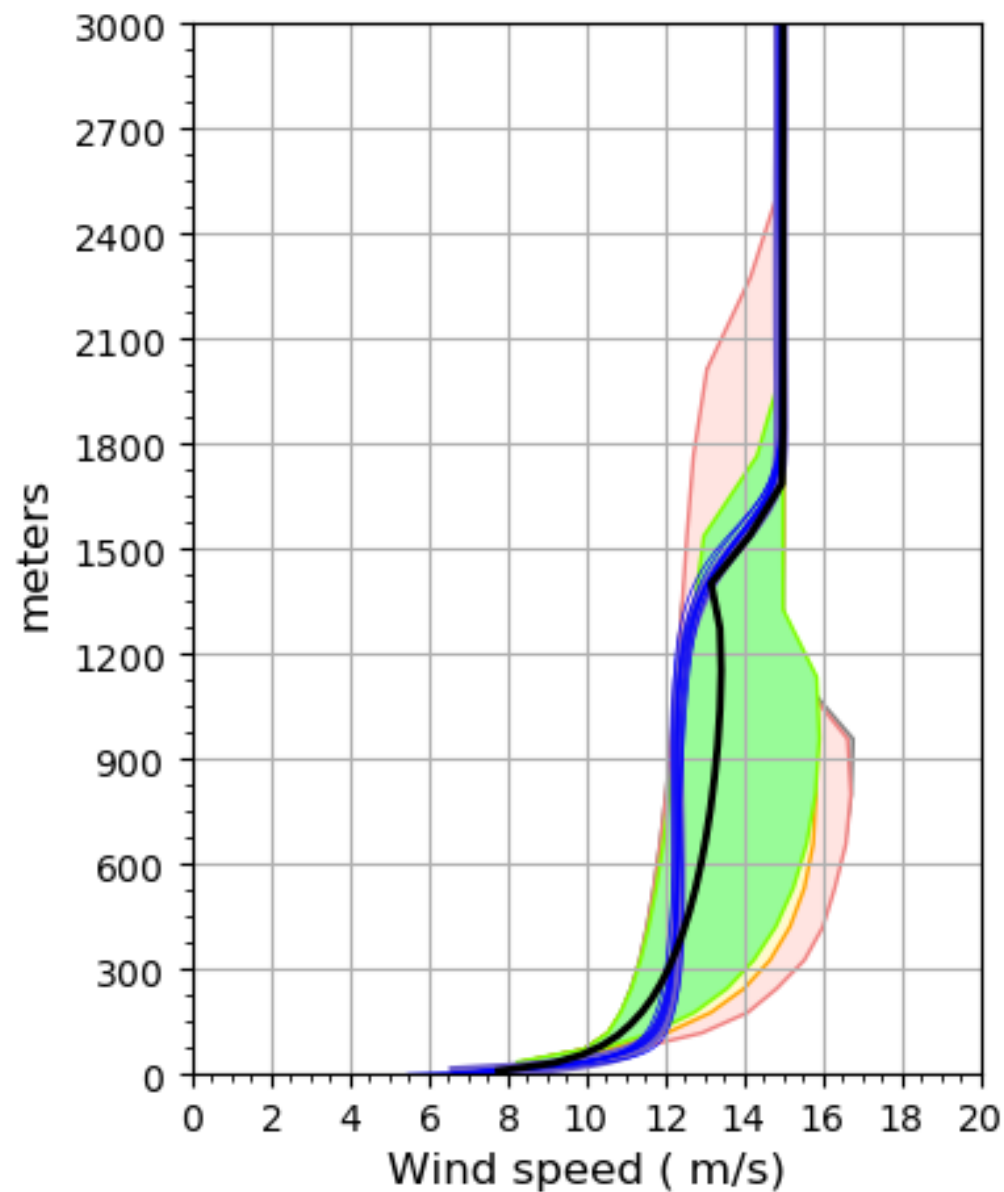


Figure 6.

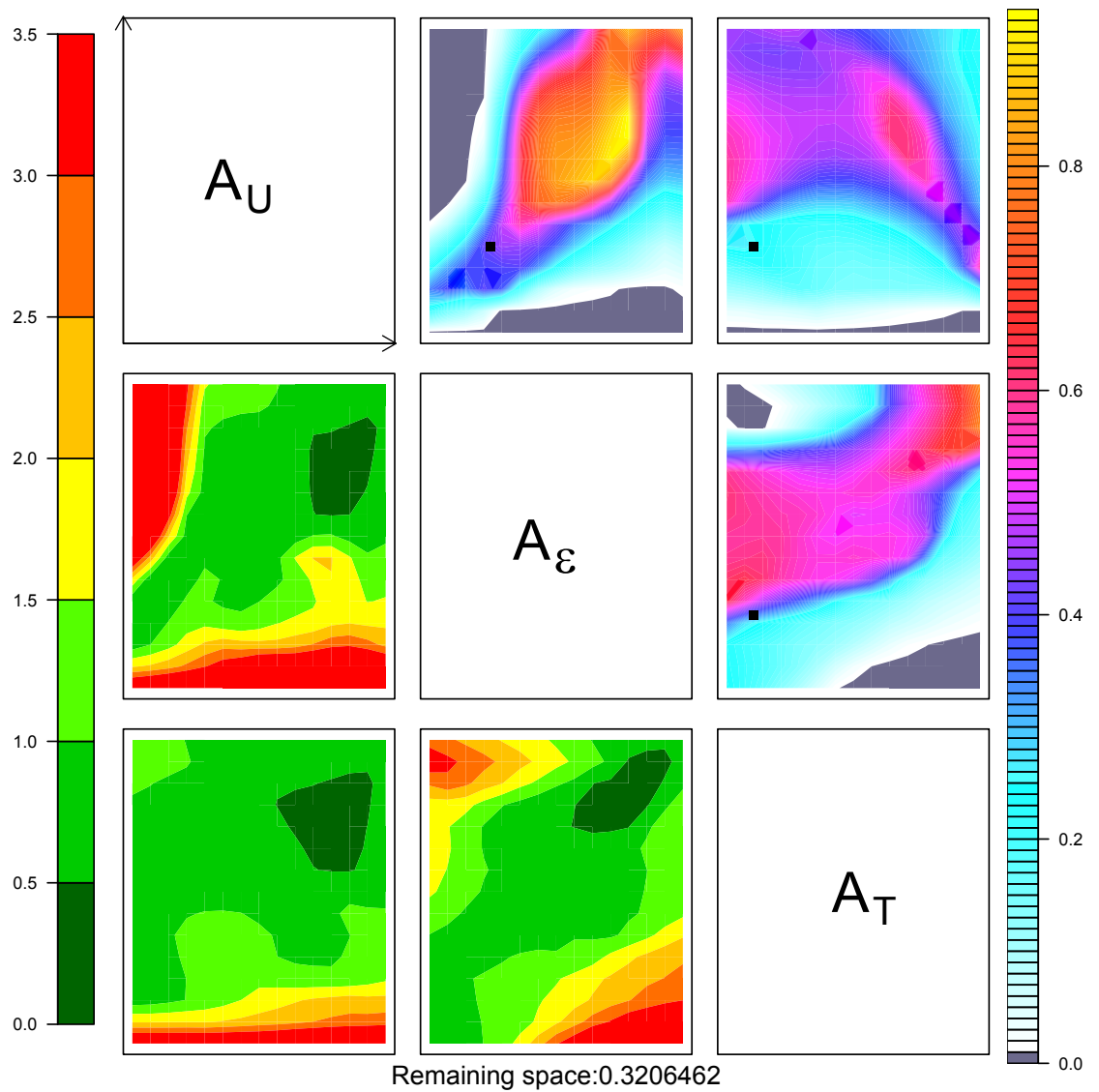
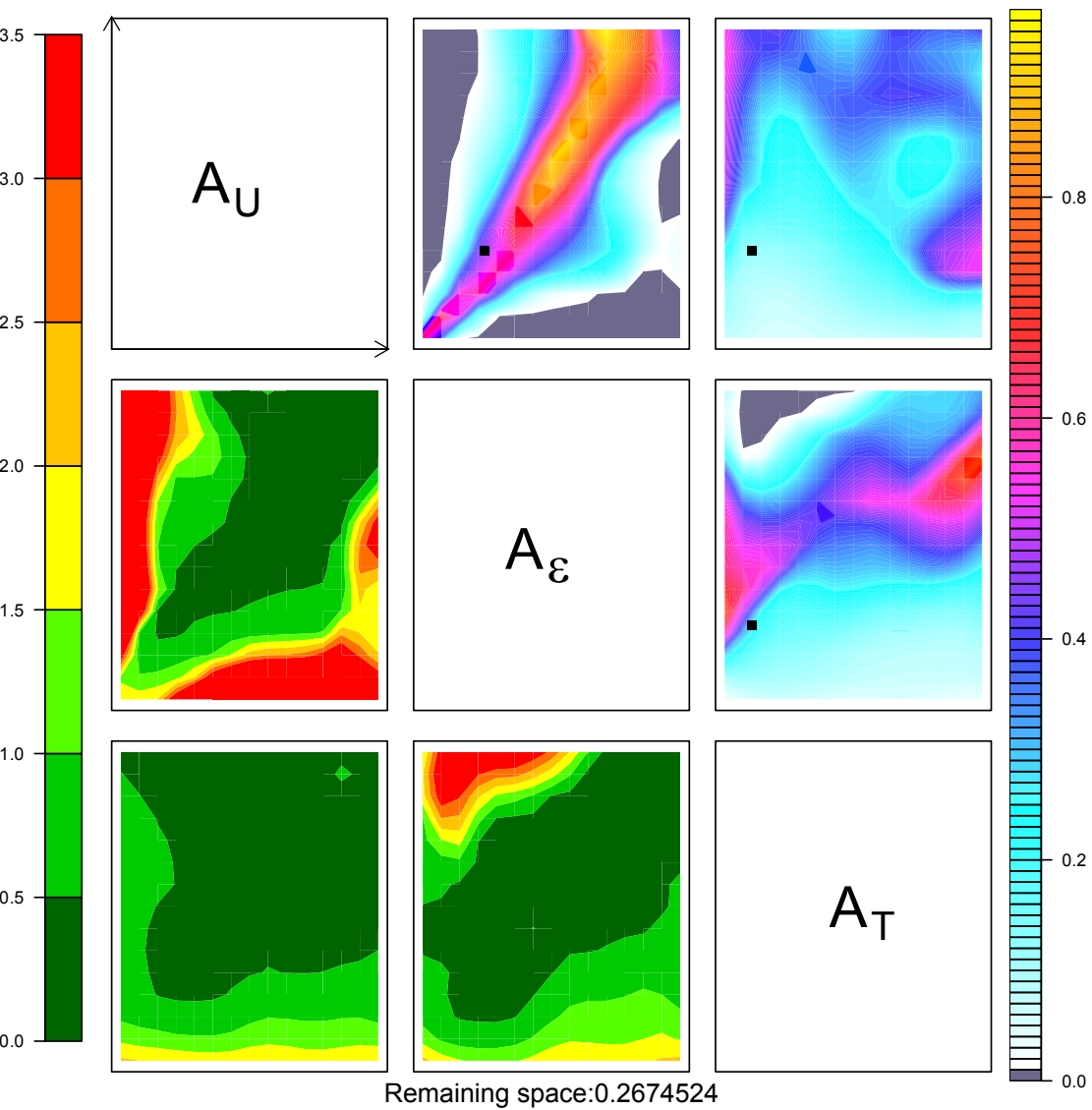
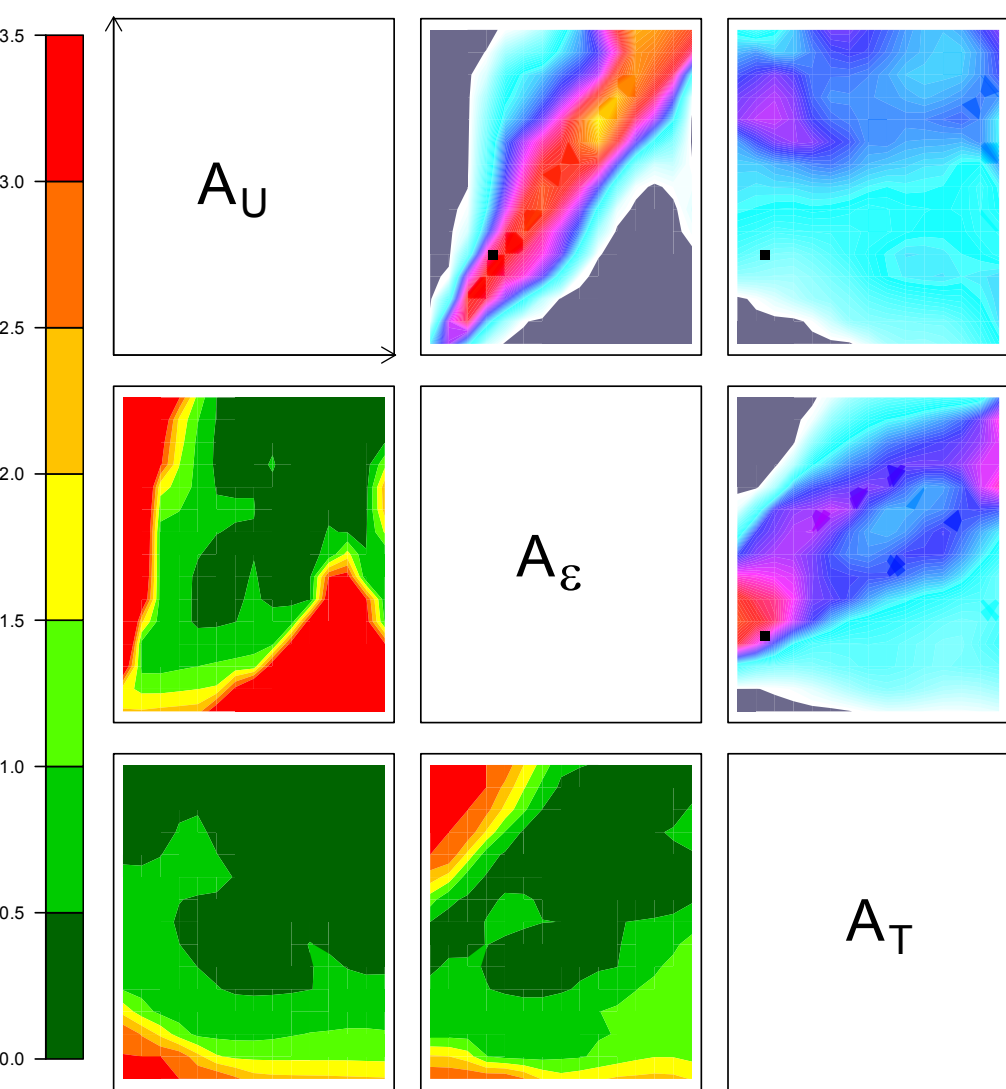
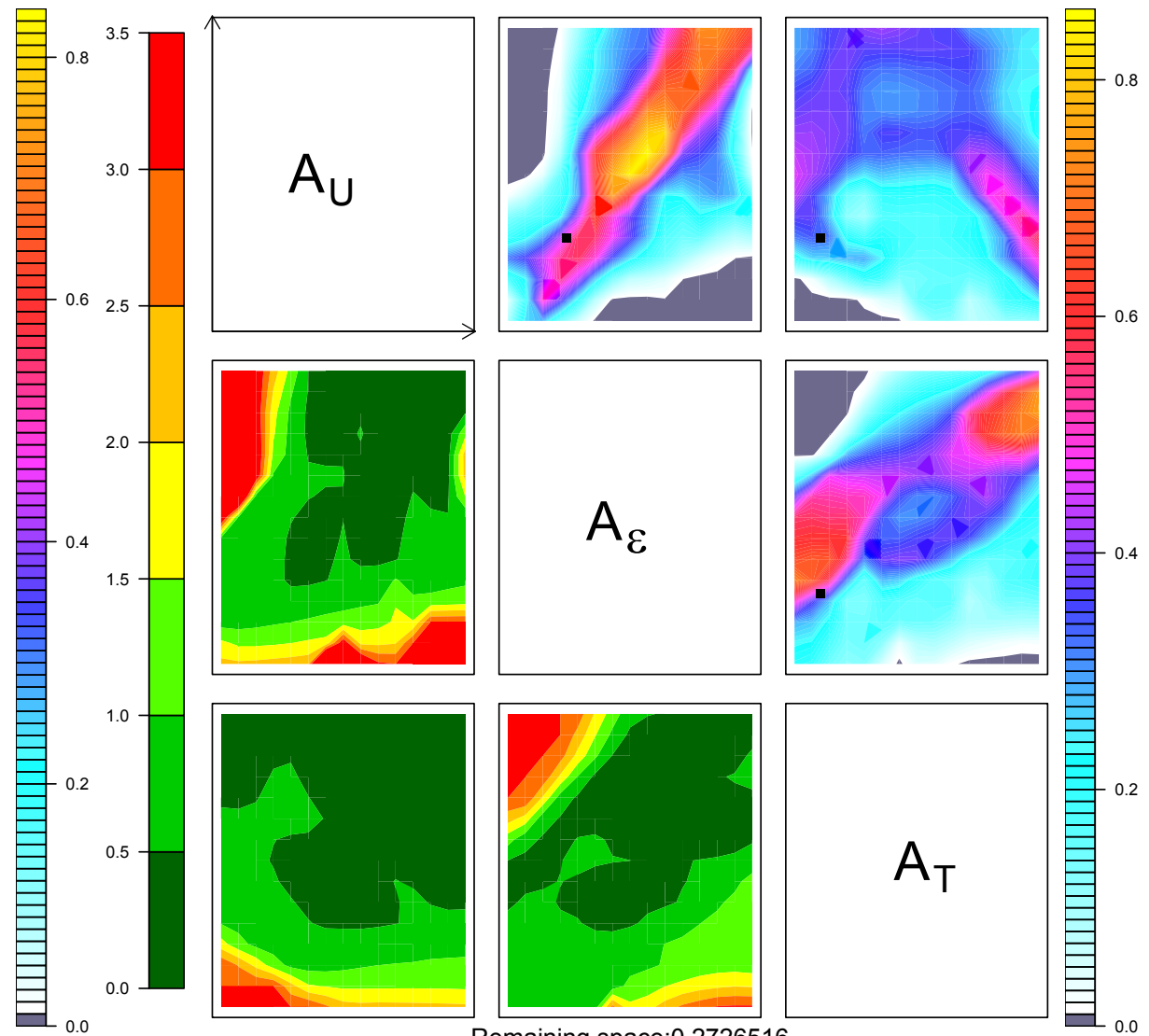


Figure 5.

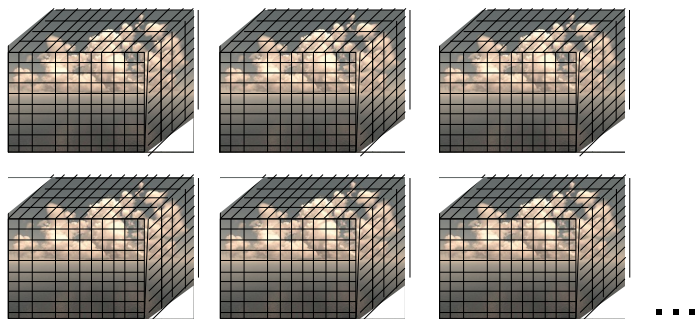
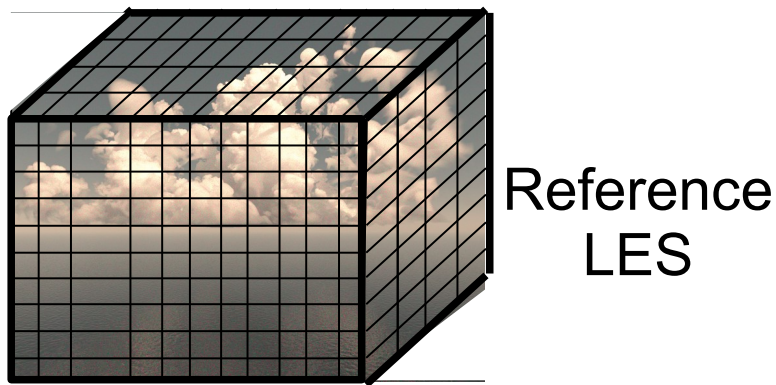


Remaining space:0.2272806



Remaining space:0.2726516

Figure 1.

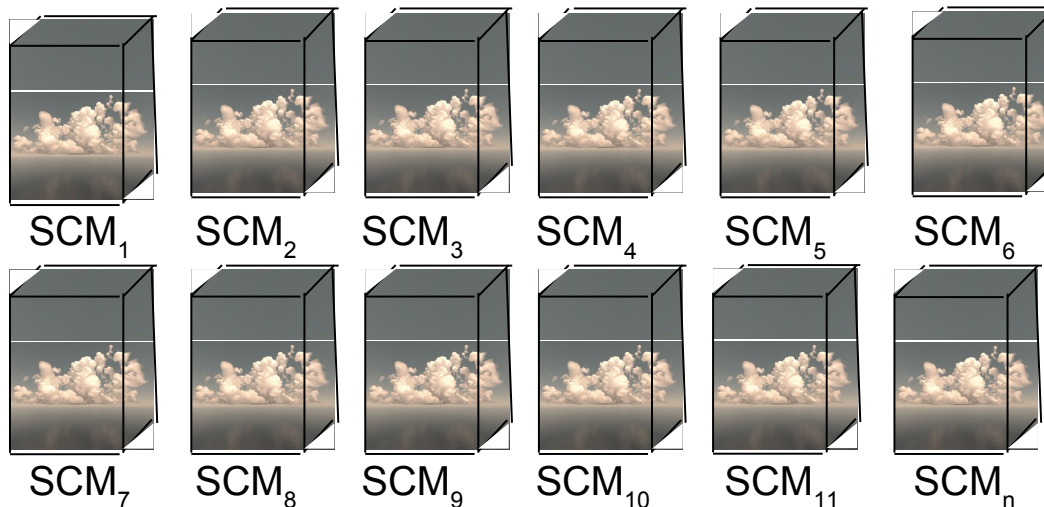


Sensitivity to resolution, domain size, parameterization option ...

1. Selection of **metrics** - **Reference metric** and **uncertainty** computed from an ensemble of LES

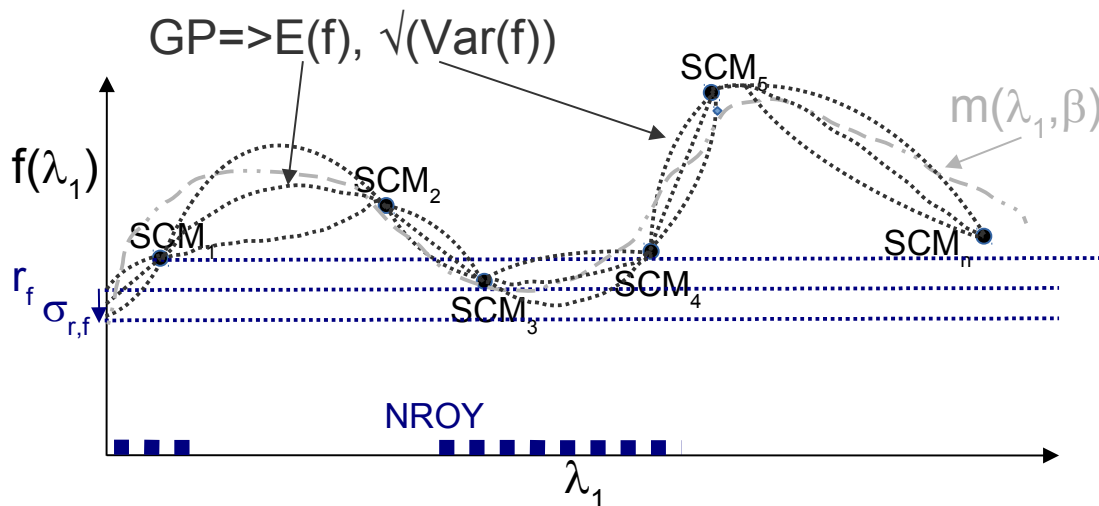
2. Identify **free parameters** and possible **range**

3. **Sample** n parameter ensemble and **run** n **SCMs**



From SCMs compute metrics

4. Build **emulator** to predict the metric for any values of parameters



5. Compare metrics to reference metric and **rule out impossible values of parameters**
 \Rightarrow Refined plausible space of parameters

Figure 3.

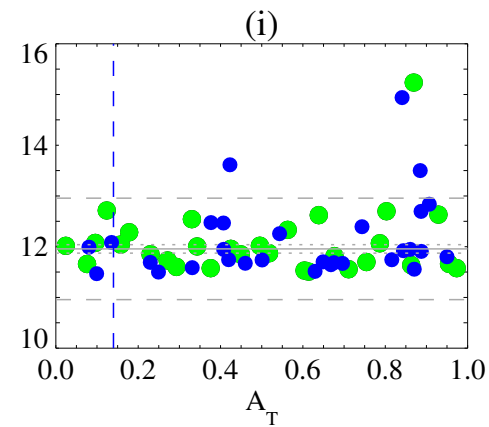
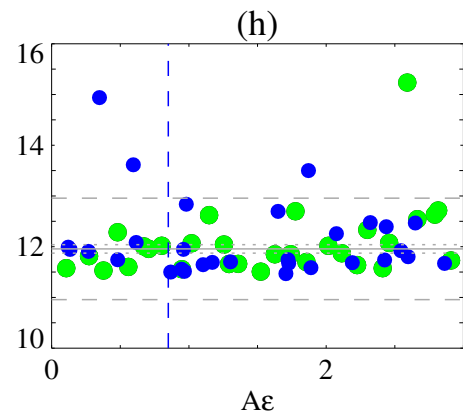
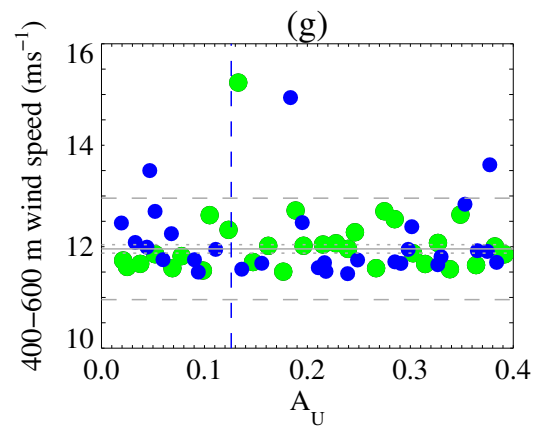
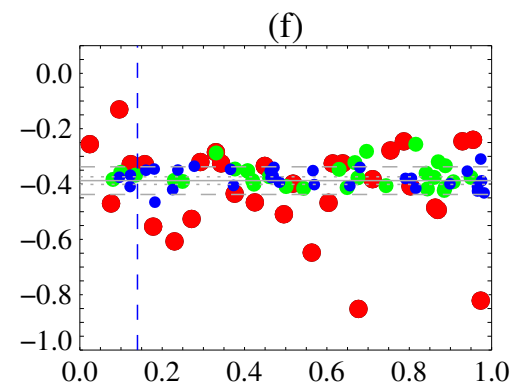
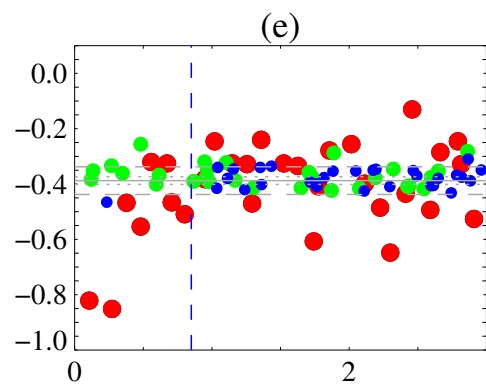
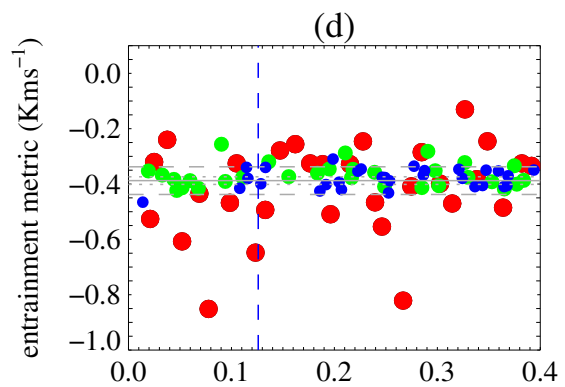
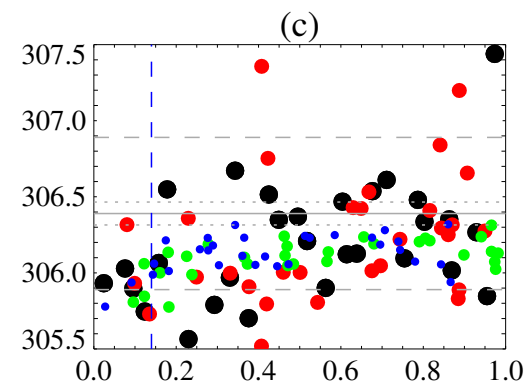
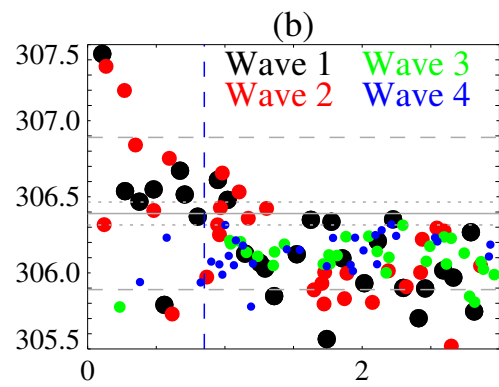
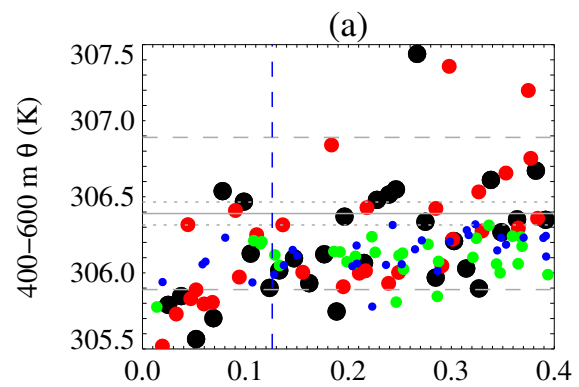
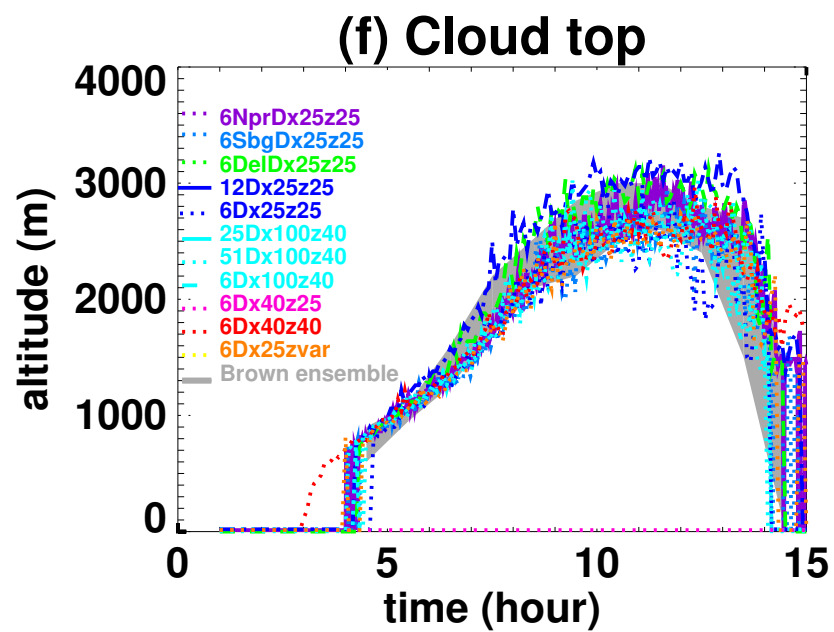
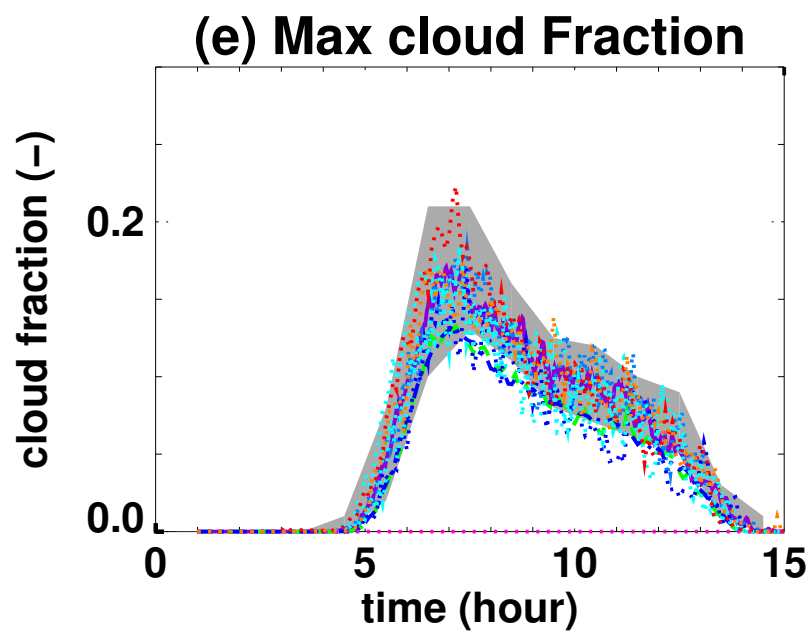
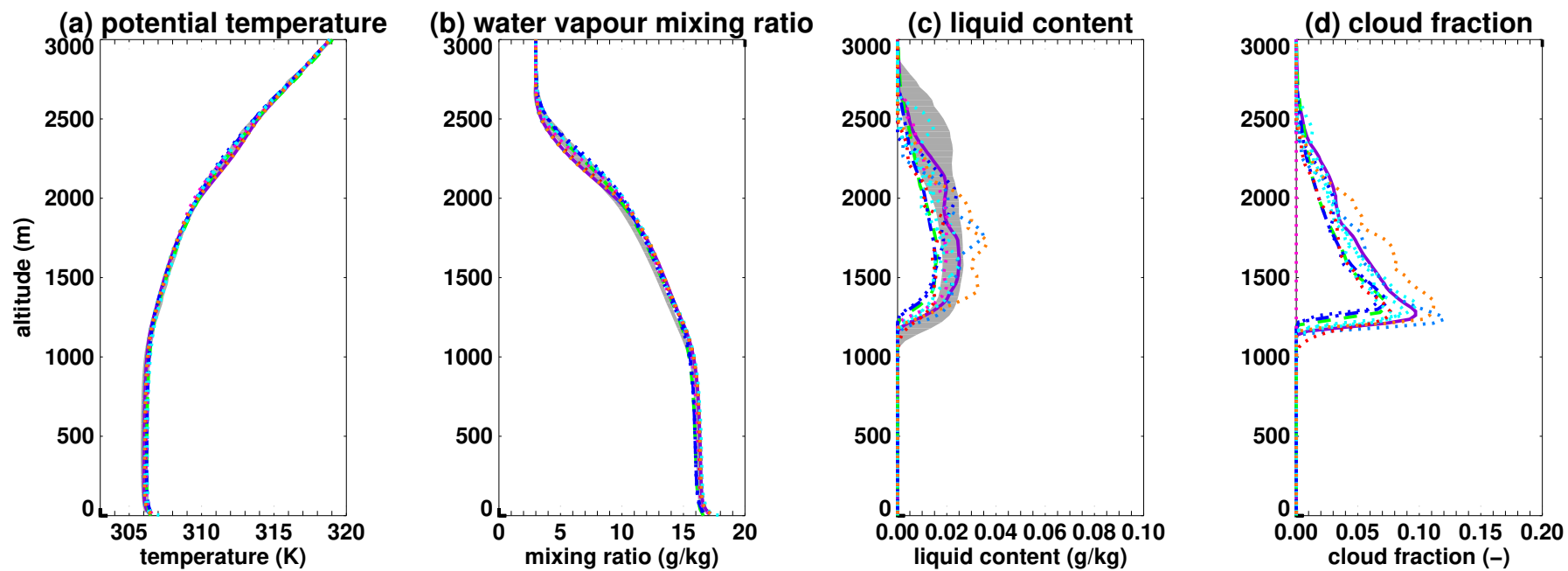


Figure 2.



Process-based climate model development harnessing machine learning: I. a calibration tool for parameterization improvement

Fleur Couvreur¹, Frédéric Hourdin², Daniel Williamson^{3,5}, Romain Roehrig¹, Victoria Volodina⁵, Najda Villefranque^{1,4}, Catherine Rio¹, Olivier Audouin¹, James Salter^{3,5}, Eric Bazile¹, Florent Brient¹, Florence Favot¹, Rachel Honnert¹, Marie-Pierre Lefebvre^{1,2}, Jean-Baptiste Madeleine², Quentin Rodier¹, Wenzhe Xu³

¹CNRM, University of Toulouse, Meteo-France, CNRS, Toulouse, France

²LMD-IPSL, Sorbonne University, CNRS, 4 pl Jussieu, Paris, France

³Exeter University, Exeter, United Kingdom

⁴LAPLACE, University of Toulouse, CNRS, Toulouse, France

⁵The Alan Turing Institute, 96 Euston Road, London, United Kingdom

Key Points:

- We apply Uncertainty Quantification to Single-Column Model/LES comparison to calibrate free parameters
- We revisit model development strategy with an emphasis on processes for model calibration
- The proposed tuning tool allows to formalize the complementary use of multicases with various metrics

A major task in the development of atmospheric models is the development of parameterizations to account for processes not resolved by the dynamical core. The improvement of model is slow partly due to the difficulty of encompassing key processes into parameterizations and because parameterizations contain ‘free’ parameters that must be calibrated or ‘tuned’. Considering the number of parameters in a model, their calibration is a complicated task, generally done manually. Recently, machine learning has been proposed as a replacement for these parameterizations. However, when models are

Corresponding author: Fleur Couvreur, fleur.couvreur@meteo.fr

28 to be used for long-term projections, exploring states far from the training data, sole use
29 of machine learning might be dangerous. It also seems counter-intuitive to replace our
30 strong physical understanding with unconstrained systems. Our proposition consists in
31 retaining parameterizations but adjoining new tools relying on machine learning to ac-
32 celerate model development. In particular we use Gaussian process-based methods from
33 uncertainty quantification to calibrate the free parameters at a process level. To achieve
34 this, we focus on the comparison of single-column simulations and reference large-eddy
35 simulations over multiple boundary-layer cases. This paper describes the tools and the
36 philosophy of tuning in single-column mode. Part 2 emphasizes how this framework can
37 help accelerate model development.

38 **Abstract**

39 The development of parameterizations is a major task in the development of weather and
 40 climate models. Model improvement has been slow in the past decades, due to the dif-
 41 ficulty of encompassing key physical processes into parameterizations, but also of cal-
 42 ibrating or ‘tuning’ the many free parameters involved in their formulation. Machine learn-
 43 ing techniques have been recently used for speeding up the development process. While
 44 some studies propose to replace parameterizations by data-driven neural networks, we
 45 rather advocate that keeping physical parameterizations is key for the reliability of cli-
 46 mate projections. In this paper we propose to harness machine learning to improve phys-
 47 ical parameterizations. In particular we use Gaussian process-based methods from un-
 48 certainty quantification to calibrate the model free parameters at a process level. To achieve
 49 this, we focus on the comparison of single-column simulations and reference large-eddy
 50 simulations over multiple boundary-layer cases. Our method returns all values of the free
 51 parameters consistent with the references and any structural uncertainties, allowing a
 52 reduced domain of acceptable values to be considered when tuning the 3D global model.
 53 This tool allows to disentangle deficiencies due to poor parameter calibration from in-
 54 trinsic limits rooted in the parameterization formulations. This paper describes the tool
 55 and the philosophy of tuning in single-column mode. Part 2 shows how the results from
 56 our process-based tuning can help in the 3D global model tuning.

57 **1 Introduction**

Atmospheric global or regional circulation models used either for numerical weather prediction (NWP) or climate studies encompass a dynamical core and a physical component. The dynamical core computes the spatio-temporal evolution of atmospheric state variables by solving a discrete version of the fluid dynamic equations. The physical component quantifies the impact on the resolved variables of radiative, thermodynamical and chemical processes, as well as dynamical processes that occur at scales smaller than the computational grid. These processes are handled by a suite of sub-models, most often referred to as parameterizations, which provide source terms in the resolved-scale equations. Parameterizations (e.g., turbulence, convection, radiation, microphysics) are often based on a mixture of physical principles and heuristic description of the involved processes, of their interactions and of their impact on the larger resolved scales. Although it is difficult to trace back the origin of the term “parameterization” in climate modelling,

it semantically points to the fact that the sub-models summarize the processes as functions of the model state vector \mathbf{x} (typically the value of zonal and meridional wind, surface pressure, temperature and water phases at each point of the 3D model grid) that depends on some free parameters. These free parameters arise from the simplification of the complex nature of the subgrid processes (e.g., assuming a bulk thermal plume instead of a population of plumes, stationarity). The atmospheric model can be summarized as

$$\frac{\partial \mathbf{x}}{\partial t} = \mathcal{D}(\mathbf{x}) + \sum_p \mathcal{P}_p(\mathbf{x}, \boldsymbol{\lambda}_p) \quad (1)$$

58 where \mathcal{D} stands for the discretized form of the fluid dynamic equations, \mathcal{P}_p for the source
 59 term provided by the parameterization of the process p and $\boldsymbol{\lambda}_p$ for the associated free
 60 parameters. This equation may however be too simplistic, as, in reality, a given parameterization
 61 often depends on intermediate variables provided by other parameterizations
 62 (e.g., cloud fraction used in radiation, turbulence variance used in the cloud scheme) and
 63 computes additional prognostic variables (e.g., turbulence kinetic energy). Nevertheless,
 64 with this simplified framework, improving models through parameterization development
 65 means both to propose more appropriate functional forms \mathcal{P}_p and to identify acceptable
 66 or better values of the free parameters $\boldsymbol{\lambda}_p$.

67 Among the different parameterizations, those involved in the representation of turbulence,
 68 convection and clouds still challenge state-of-the art NWP and climate models (Holtslag et al.,
 69 2013; Nam et al., 2012; Nuijens et al., 2015; Klein et al., 2017; Randall et al., 2003;
 70 Bony et al., 2015). Innovative and diverse concepts and ideas have been proposed over the
 71 past decade to improve this representation (Rio et al., 2019). A detailed understanding of
 72 the physical processes leading to the formation of low-level clouds can be obtained by Large-
 73 Eddy simulations (LES) (Guichard & Couvreux, 2017), which reproduce, with high fidelity,
 74 the turbulent dynamics within the clouds (e.g., Siebesma & Cuijpers, 1995; Neggers,
 75 Duijkerke, & Rodts, 2003; Wang & Feingold, 2009). LES are therefore increasingly used to
 76 derive and evaluate the conceptual models at the root of boundary-layer and shallow cloud
 77 parameterizations. The choice of the parameterization free parameters is also crucial for the
 78 simulation of clouds. Their calibration or “tuning” consists in searching for acceptable or
 79 optimal values of these parameters, such that the associated model configuration has a
 80 realistic behavior under various conditions and compared to a suite of observations (Mauritsen
 81 et al., 2012). Calibration is therefore a fundamental aspect of NWP or climate model
 82 development. However, it is often

83 conducted without much control on the way it modifies the parameterization behavior
84 at the process level as the calibration focuses more on regional or global constraints, such
85 as the radiative balance of the Earth System for climate models, or performance met-
86 rics (e.g. root mean square error, skill scores) for NWP models. Hourdin et al. (2017)
87 compile the tuning strategies of several climate groups and emphasize that most of the
88 parameters used to tune climate models (droplet size, fall velocity, entrainment rate) are
89 related to clouds (see also Golaz et al., 2013), i.e. the most uncertain processes that af-
90 fect radiation, the primary engine of the atmospheric circulation.

91 Given the societal needs for reliable climate simulations and weather forecasts, the
92 progress achieved by the global atmosphere modeling community has been found slow
93 (Jakob, 2010). Several systematic errors in state-of-the-art models have been modestly
94 reduced, such as those regarding the surface temperature over the eastern oceans (Richter,
95 2015), the rainfall distribution in the Tropics (Flato et al., 2013), the variability of the
96 liquid water path (Jiang et al., 2012) and the low clouds (Nam et al., 2012). The dead-
97 lock of the cloud parameterization, highlighted by Randall et al. (2003), is still an issue
98 today. This too slow improvement of models can be attributed to remaining deficiencies
99 in the structure of the parameterization itself (the function \mathcal{P}_p) but also to the calibra-
100 tion of model parameters that can be considered as a bottleneck in model development.
101 On the one hand, the calibration may not be done efficiently enough, and on the other
102 hand, tuning may induce error compensations that contribute to slow model develop-
103 ment. Indeed, a new model development usually starts with a model score degradation
104 by breaking this compensation, as often experienced in the weather prediction centers
105 where strong weight on well-established metrics slows down the implementation of new
106 model development in the operational version (Sandu et al., 2013).

107 Various avenues have been proposed to get around these difficulties and acceler-
108 ate climate model improvement. A first avenue seeks to exploit the high resolution, ex-
109 plicitly resolving convection, to reduce the number of involved parameterizations. With
110 the recent increase of computer power, it is nowadays possible to run global kilometer-
111 scale resolution simulations over a few months (Satoh et al., 2008, 2019; Stevens et al.,
112 2019). However, the explicit simulation of the fluid dynamics associated with the life cy-
113 cle of a cumulus requires grid resolution of the order of several tens of meters. Such res-
114 olution will not be accessible in the foreseeable future for climate change projections which
115 require simulations of the global Earth System covering at least several hundreds of years

116 (model spin-up plus transient simulations in response to anthropogenic forcing). The super-
117 parameterization approach (Randall et al., 2003) proposes an intermediate pathway by
118 introducing a convection-permitting model in each column of a conventional general cir-
119 culation model (GCM) to replace the deep convection parameterization (Khairoutdinov
120 et al., 2005). The use of a large-eddy model instead of a convection-permitting model
121 in such framework further removes the boundary-layer and shallow convection param-
122 eterizations (Grabowski, 2016; Parishani et al., 2017). A second avenue recently explored
123 the potential of machine learning approaches, which ultimately envisions to replace some
124 parameterizations by neural networks or similar algorithms, properly trained on convection-
125 permitting model simulations or superparameterized GCM (Krasnopolsky et al., 2013;
126 Brenowitz & Bretherton, 2018; Gentine et al., 2018).

127 A third proposition consists in retaining parameterizations in models but adjoin-
128 ing new tools relying on machine learning to accelerate model development. This choice
129 is motivated by the fact that parameterizations summarize our current understanding
130 of the dynamics and physics of atmospheric processes and offer the power of interpre-
131 tation, crucial to build our confidence in the extrapolation beyond observed conditions
132 realized by any climate projections. The ESM2.0, proposed by Schneider et al. (2017),
133 belongs to this category. The authors defend that the major progress in Earth-System
134 model development should come from a more systematic use of global observations and
135 high-resolution simulations thanks to machine learning algorithms. They also underline
136 the importance of climate model calibration. In particular, they stress that their new
137 Earth System modeling framework comes with challenges such as developing innovative
138 learning algorithms, identifying the best metrics, combining information from observa-
139 tions and high-resolution, innovating in the design of parameterizations such that they
140 can more easily benefit from new observations or evolution of the models (e.g., refine-
141 ment of resolution).

142 Along the same lines, we propose, in this paper, a new approach which allows the
143 development of the parametrizations and their calibration to be tackled at the same time.
144 We argue that a major slowdown of model improvement resides in the difficulty to clearly
145 identify parameterization deficiencies and to properly disentangle them from the inher-
146 ent calibration of their adjustable parameters at the process and global scales. It is likely
147 that process-scale parameterization improvements are often hidden by the unavoidable
148 full model retuning, required to maintain a reasonable radiative balance or acceptable

149 scores. In the proposed approach, machine learning is harnessed in a principled way to
150 calibrate parameterizations at process level. We promote a more systematic use of the
151 multi-case comparison between Single-Column Model (SCM) and LES to evaluate and
152 calibrate parameterizations, as we advocate that a lot still remains to be learnt from this
153 comparison. Such a systematic use is not feasible however without more objective and
154 automatic methods than the traditional trial/error approach used to fix parameter val-
155 ues during the parameterization development. Indeed, this trial/error approach is only
156 applicable to one piece of a particular parameterization and one or two relevant cases
157 at most. Here, we aim at assessing a set of parameterizations \mathcal{P}_p for a series of test cases,
158 which can be formalized as the question of the existence of a sub-space of the param-
159 eters λ_p that allows to match metrics between SCM and LES results for the series of cases,
160 within a given tolerance to error.

161 Hourdin et al. (2017) reviewed the general practice for climate model calibration
162 and proposed three different levels of calibration in a model development: a first cali-
163 bration at the level of individual parameterizations, then a calibration of each compo-
164 nent of the Earth System model and eventually a calibration of the full Earth System
165 model. Distinguishing those three levels may avoid compensating errors that could arise
166 if the calibration is only done at the last level. In this paper, we propose a methodol-
167 ogy to address the first phase, *i.e.* the process-level calibration and defend that it can
168 be part of the elaboration of a well-defined calibration strategy based on solid physical
169 and statistical methodologies. By doing so, we tackle model development and param-
170 eter calibration together rather than independently as currently done for most climate
171 model development.

172 Machine learning has already been proposed to calibrate free parameters (e.g., en-
173 semble Kalman filters as in Schneider et al., 2017). The methodology retained here for
174 model calibration uses history matching with Gaussian processes. History Matching is
175 an efficient way to explore and reduce the domain of free parameters λ_p and document
176 how a model physics, namely the suite of functions \mathcal{P}_p , behaves within this domain. Williamson
177 et al. (2013) applied History Matching to tune the Hadley Climate Model and stressed
178 its advantage: it accounts for the various sources of uncertainties in assessing the com-
179 patibility of the model with the reference: namely the reference uncertainty itself, the
180 uncertainty introduced by the Gaussian process representation of the parametrization,
181 and the intrinsic ability of the model to represent the reference (often referred to as struc-

182 tural error or model discrepancy). History matching inherently deals with the overcon-
183 fidence issue, which emerges when model calibration is addressed as an optimization prob-
184 lem (Salter et al., 2019). It has been widely used to calibrate models in astrophysics (Vernon
185 et al., 2010), epidemiology (Andrianakis et al., 2017) and hydrocarbon reservoirs (Craig
186 et al., 1996). It has been applied to climate models (Williamson et al., 2015, 2017) and
187 is starting to be used to find biases in models (McNeall et al., 2019).

188 Whilst history matching has been applied to calibrate 3D models, it has not been
189 harnessed for process-level tuning, as we advocate here through application to SCM/LES
190 comparison. The SCM approach provides confidence in the model’s ability to represent
191 some of the key processes whereas a direct calibration of the 3D global model targeting
192 large-scale constrains may hide compensating errors (as discussed in Williamson et al.,
193 2017). SCM calibration is able to reduce the domain of the free parameters for a param-
194 eterization, information that can be used for efficiently calibrating the full 3D global model
195 (as we demonstrate in part II). The breakthrough proposed here was only possible thanks
196 to a strong collaboration between the Uncertainty Quantification community and the at-
197 mospheric modelers.

198 The present paper focuses on parameterizations involved in the representation of
199 boundary-layer clouds. Indeed, well-established case studies exist for such regimes and
200 LES have been shown to realistically represent the main processes. However, this method-
201 ology can be easily expanded to other parameterizations and other objectives in the Earth
202 System.

203 The paper is organized as follows: the next section describes the SCM/LES frame-
204 work highlighting its advantages, recalls the different steps used in the development of
205 a parameterization and details the new philosophy advocated here. Section 3 presents
206 the statistical tool, with a focus on its philosophy and its main ingredients. Section 4
207 presents a guideline for its use based on a simple illustration. The paper ends with con-
208 clusions in Sect. 5. A companion paper (part II) illustrates the significant advances in
209 model development offered by this tool. It exploits process-based calibration for model
210 development and shows how this tool provides guidance for the tuning of a 3D global
211 model.

212 **2 A systematic use of the SCM/LES comparison**

213 Observations only provide a sparse view, in time, space and variables, of the phys-
 214 ical processes responsible for convection and clouds. In contrast, LES have the advan-
 215 tage of providing coherent 3D fields characterizing the dynamical and thermodynami-
 216 cal state of the atmosphere. Of course, LES models include turbulence and microphysics
 217 parameterizations and thus contain modeling uncertainties, but they have been shown
 218 to reproduce the turbulent dynamics of the clouds with high fidelity (e.g., Neggers, Duynkerke,
 219 & Rodts, 2003; Heus et al., 2009). As a result, LES have become a central tool in the
 220 development and evaluation of parameterizations of convection and clouds. Their anal-
 221 ysis has helped in building the conceptual models behind several parameterizations (e.g.,
 222 Neggers et al., 2002; Rio et al., 2010). LES are also used for the evaluation of the pa-
 223 rameterizations in particular those involved in the representation of boundary layers and
 224 shallow clouds (e.g., Ayotte et al., 1996; Golaz et al., 2002; Hourdin et al., 2002; Neg-
 225 gers et al., 2004; Siebesma et al., 2007; Rio & Hourdin, 2008; Caldwell & Bretherton, 2009;
 226 Neggers, 2009; Pergaud et al., 2009; Rio et al., 2010; Suselj et al., 2013; Neggers et al.,
 227 2017; Tan et al., 2018; Suselj et al., 2019).

For their evaluation, parameterizations are often tested in a single-column frame-
 work, particularly relevant for global circulation model parameterizations, which are fun-
 damentally 1D. SCM are built by extracting, from a 3D model, a single atmospheric col-
 umn, which integrates the same set of subgrid parameterizations (boundary-layer, shal-
 low convection, deep convection and microphysics schemes) and is run in a constrained
 large-scale environment (Zhang et al., 2016). The state vector of the SCM simulation
 is then a restriction to one column \mathbf{x}_c of the full 3D state vector \mathbf{x} and Eq. 1 reduces
 to Eq. 2. The dynamical term $\mathcal{D}(\mathbf{x})$ becomes a source term \mathcal{F}_c specified as a function
 of time and altitude z ; we however discard this dependency in the notation for simplic-
 ity. It can also depend on the column full state vector, $\mathcal{F}_c(\mathbf{x}_c)$, if for instance the large-
 scale advection is separated between a prescribed horizontal advection and a vertical ad-
 vection computed as $-w\partial\mathbf{x}_c/\partial z$, where w is an imposed vertical velocity. During the SCM
 integration, some parameterizations can be deactivated in which case the correspond-
 ing source term is either neglected or included in the forcing \mathcal{F}_c . It is the case for instance
 when the radiative heating is imposed rather than being computed interactively by the
 model radiation scheme or when turbulent surface fluxes are imposed rather than com-
 puted by the model bulk parameterizations. What really matters in the SCM/LES approach

is that both models use the exact same initial and boundary conditions and forcing terms. In a simplified formalism, the SCM thus corresponds to

$$\frac{\partial \mathbf{x}_c}{\partial t} = \sum_{P_{\text{activated}}} \mathcal{P}_p(\mathbf{x}_c, \lambda_p) + \mathcal{F}_c(\mathbf{x}_c) \quad (2)$$

and the LES to

$$\frac{\partial \mathbf{y}}{\partial t} = \mathcal{L}(\mathbf{y}) + \mathcal{F}_c(\bar{\mathbf{y}}) \quad (3)$$

with

$$\mathbf{x}_c(t = 0) = \bar{\mathbf{y}}(t = 0) \quad (4)$$

228 where \mathbf{y} stands for the full LES state vector, $\mathcal{L}(\mathbf{y})$ to the LES model equations (which
 229 include the LES parameterizations) and $\bar{\mathbf{y}}$ to the horizontal-domain average of the LES
 230 state vector. The SCM/LES framework thus provides a rigorous comparison between
 231 both simulations, as it removes the uncertainties, which may arise from different initial
 232 conditions or large-scale forcing when directly comparing SCM to observations. This con-
 233 strained framework avoids the need to disentangle parameterization contributions from
 234 their coupling with the large-scale dynamics. Another important aspect of the method
 235 is that SCM simulations are computationally very cheap. The joint utilization of LES
 236 and SCM was first advocated by Randall et al. (1996); Ayotte et al. (1996) and has been,
 237 since then, widely used within the Global Energy and Water Exchanges (GEWEX) Cloud
 238 System Study (GCSS; Browning et al. (1993) community, now renamed the Global At-
 239 mospheric System Studies, GASS, community). One of the most important legacies of
 240 this group for the atmospheric modeling community is an ensemble of test cases that con-
 241 nect observations, LES and SCM, and which sample many typical situations over the globe,
 242 thought to be of importance for the climate system (e.g., Siebesma & Cuijpers, 1995;
 243 Brown et al., 2002; Duynkerke et al., 2004). As such, this framework has been increas-
 244 ingly used in model development (e.g., Hourdin et al., 2013; Gettelman et al., 2019; Hour-
 245 din et al., 2020; Roehrig et al., 2020), all the more so as SCM simulations have been shown
 246 to reproduce uniquely the behaviour of their GCM justifying the use of SCM simulations
 247 for improving weather and climate models (Hourdin et al., 2013; Neggers, 2015; Gettel-
 248 man et al., 2019).

249 Traditionally, parameterizations are often tested over a few specific cases for which
 250 high-resolution simulations are available (e.g., Ayotte et al., 1996). Recently, the im-
 251 portance of using a wide benchmark of cases covering the different regimes encountered
 252 in reality instead of only a limited number of cases has been stressed (e.g., Neggers et

253 al., 2012). We also highlight here the importance of using an extensive ensemble of cases.
254 The use of multi-case is indeed essential for exploring the various degrees of freedom of
255 the parameterization package. A stable boundary-layer case will constrain the turbulent
256 diffusion; the combination of cloud free and cumulus topped convective boundary lay-
257 ers will ensure that cloud cover is obtained for a good representation of convection; tran-
258 sition cases from stratocumulus to cumulus will ensure the extension to stratocumulus
259 regimes, etc. Combining multi cases and multi metrics is a much more robust assessment
260 of model performance as also highlighted by (Neggers et al., 2017). To better use multi-
261 cases, one important technical aspect is a common definition, in a predefined acknowl-
262 edged format, for the description of the setup of reference cases, to be used both to per-
263 form SCM simulations or LES. This definition should include the description of the ini-
264 tial profiles and large-scale forcing but also contain information on the configuration to
265 be used (e.g. the type of surface boundary conditions, the existence of any nudging to-
266 wards reference vertical profiles, the way large-scale forcings are provided). An interna-
267 tional initiative is ongoing to agree on the description of the format for this definition
268 file. Sharing a standard to define cases will ease the realization of cases by any model
269 and facilitate the share of new cases. The importance of creating libraries of high-resolution
270 simulations representing different climate is another important aspect already identified
271 as a goal by the GCSS community and stressed in Schneider et al. (2017). A common
272 format and the libraries of LES are an important pre-requisite for the tool presented here.
273 In addition, both will contribute to bringing the process-scale community and the com-
274 munity developing global models more closely together.

275 When comparing SCM and LES, the modeler has to decide which metrics to con-
276 sider. Various types of metrics can be used. One can directly compare components of
277 the SCM state vector \mathbf{x}_c to their equivalent in LES, the horizontal domain-average state
278 vector $\bar{\mathbf{y}}$ (e.g., vertical profiles of potential temperature, specific humidity and less of-
279 ten wind components). Assessing the ability of the parameterizations to reproduce the
280 time evolution of \mathbf{x}_c for a given forcing is indeed the ultimate goal. By doing so, one not
281 only tests the behavior of one particular parameterization but also its coupling with the
282 other parameterizations activated in the SCM. However, it may make the determination
283 of the behavior of the targeted parameterization more difficult and can hide compensat-
284 ing errors: for example, a given temperature turbulent flux can be obtained by differ-
285 ent contributions from organized structures and small-scale turbulence when represented

286 by two different parameterizations such as in the Eddy-Diffusivity Mass-Flux framework
287 (Hourdin et al., 2002; Siebesma et al., 2007; Neggers, 2009; Pergaud et al., 2009). An-
288 other type of metrics targets parameterization-oriented variables, such as mass fluxes,
289 heating source associated with one part of the motion only, subgrid-scale distribution
290 of temperature or water, cloud vertical structure, updraft vertical velocity, area fraction
291 or entrainment and detrainment rates. The metric, from the SCM point-of-view, is no-
292 longer derived from the model state variables but corresponds to an internal variable to
293 the parameterizations. However, additional uncertainty arises from the way such vari-
294 ables and associated metrics can be derived from LES. For example, clouds can be char-
295 acterized in an LES as all the grid cells containing condensed water (e.g., Siebesma &
296 Cuijpers, 1995). Combined with thresholds on the vertical velocity, cloudy updrafts can
297 be separated from cloudy downdrafts. The analysis of the joint distribution of variables
298 (Chinita et al., 2018) or the use of ad-hoc passive tracers can also be used in the LES
299 to identify objects relevant with the conceptual model of the parameterization (e.g., Cou-
300 vreux et al., 2010; Rio et al., 2010; Chinita et al., 2018; Brient et al., 2019). Such parameterization-
301 oriented diagnostics have helped in the refinement of the conceptual model at the root
302 of the parameterization (e.g., Rio et al., 2010; Jam et al., 2013; Rochetin et al., 2014).
303 However, a question arises if such diagnostics should also be used as metrics in the cal-
304 ibration process. Answering this question on the relative importance to give to one type
305 of metrics or another requires efficient algorithms, as the one proposed here, to explore
306 the various options. Note also that using state vector-based metrics on a large set of cases
307 that are more or less sensitive to one aspect of the parameterization may help avoid the
308 error compensation issue. Neggers et al. (2017) propose to combine simple metrics on
309 a unique score metric through the use of the bias and the root-mean square errors on
310 each metric. As will be detailed later, we have decided to explicitly keep the individual
311 information brought by each metric.

312 In line with Neggers et al. (2012), we advocate that, although not a new approach,
313 the power of SCM/LES comparisons is largely underestimated and under-exploited. Ap-
314 plying history matching to this comparison is a way to fully take advantage of the SCM/LES
315 on a large multi-case ensemble and explore whether there exists a sub-space of the pa-
316 rameter space for which the SCM is able to reproduce a series of LES simulations within
317 a given uncertainty. Note that the metrics can be different from one case to the other.

318 This tool offers the possibility to revisit the different intercomparison exercises documented
 319 in the literature and to benefit from this rich database still underused.

320 Eventually, a point that becomes crucial when using LES for parameterization eval-
 321 uation and tuning is the assessment of LES reliability and its uncertainties. Although
 322 it has been shown, through the comparison to observations, that LES is able to correctly
 323 reproduce boundary-layer processes and shallow clouds (Couvreur et al., 2005; Neggers,
 324 J. & Siebesma, 2003; Heus & Jonker, 2008), LES, as in many models, come with uncer-
 325 tainties associated to the advection scheme and the parameterizations still active in such
 326 simulations concerning small-scale turbulence, microphysics, radiation and surface fluxes.
 327 Sullivan and Patton (2011) have shown that a horizontal resolution of a few tens of me-
 328 ters for convective boundary layers is enough to get convergence for the mean, fluxes and
 329 variances but 10m resolution is needed in order to get convergence on skewness. The sen-
 330 sitivity of LES of shallow convection to resolution, size of the domain, subgrid model and
 331 advection scheme has been widely investigated (Brown, 1999; Matheou et al., 2011; Pres-
 332 sel et al., 2017; Zhang et al., 2017; Wurps et al., 2020). In particular, it has been shown
 333 that most of the ensemble-averaged turbulence statistics are reasonably insensitive, al-
 334 lowing one to use LES results to develop and evaluate convection parameterizations. How-
 335 ever, some characteristics of the cloud fields (e.g. size distribution of individual clouds)
 336 are more sensitive to resolution or advection scheme (Brown, 1999; vanZanten et al., 2011).
 337 Uncertainty around this reference should be documented so that history matching can
 338 explicitly take it into account.

339 **3 *High-Tune Explorer (htexplo)*, a statistical tool to calibrate model** 340 **parameters and more**

341 **3.1 Overview**

342 The present section describes the tool proposed to perform process-based calibra-
 343 tion. Its objective is twofold: (i) characterize the domain of the model parameter val-
 344 ues that allows the model to appropriately capture process-level metrics and which can
 345 be used for subsequent calibration of the global model, and (ii) identify the model pa-
 346 rameters that limit model performance and thus highlight the need for model param-
 347 eterization revision. The tool relies on history matching approach developed by Vernon
 348 et al. (2010) and first used for climate studies by Williamson et al. (2013). This method
 349 aims at removing “unphysical” regions of parameter space iteratively, refocusing the search

350 for “acceptably tuned” models at each step. The tool finds the subspace of the model
 351 parameter space containing simulations consistent with the reference metrics, acknowl-
 352 edging the various sources of uncertainty. This tool has already been successfully applied
 353 to identify the acceptable range of model parameter values in the 3D configuration of
 354 the Hadley Centre climate model (Williamson et al., 2013, 2015) or in the NEMO oceanic
 355 model (Williamson et al., 2017). It is here used for the first time in the context of the
 356 SCM/LES comparison for a given set of cases.

357 As already stated in the previous section, we focus here on the parameterizations
 358 involved in the representation of boundary-layer clouds (turbulence, convection, cloud
 359 micro and macrophysics, radiation). However, this methodology can be easily expanded
 360 to other parameterizations and other objects of the Earth system as soon as reliable ref-
 361 erences are available.

362 Figure 1 sketches the main steps of the *High-Tune Explorer* (htexplo in the follow-
 363 ing for an explorer to use High-resolution simulation to improve and Tune parameter-
 364 izations) tool:

- 365 • **1. Metric selection and references** First, the cases and associated target met-
 366 rics are selected. The relevant reference for each metric is then identified and the
 367 associated uncertainty is estimated. In the present case, the reference is an LES
 368 and the associated uncertainty is based on an LES ensemble. Observations could
 369 also be used with an associated error when an LES is not available. This phase
 370 is not model-specific and could be shared between different models.
- 371 • **2. Selection of model parameters** The model parameters to be calibrated are
 372 identified and their possible range of values are determined.
- 373 • **3. Experimental design and SCM runs** The experimental design consists of
 374 defining the ensemble of experiments (or SCM) to be run. The goal is to optimally
 375 sample the parameter space and provide a small set of parameter values for which
 376 the single-column model will be run. Metrics are computed from each of the SCM
 377 simulations and form the training data-set on which emulators are built.
- 378 • **4. Building emulators**, i.e. construction of surrogate models, also called “em-
 379 ulators”, one for each metric. Each emulator is based on a Gaussian Process (GP)
 380 and predicts the corresponding metric value at any point of the full parameter space,
 381 without running the SCM. The GP statistical model also provides a probability

382 distribution of its prediction, thus quantifying the prediction uncertainty for use
 383 in calibration.

- 384 • **5. History matching** The comparison between the reference metrics and those
 385 inferred with the emulators is based on a distance that accounts for reference un-
 386 certainty, modeler tolerance to error or model discrepancy (induced by e.g., mis-
 387 representation of specific processes, inaccuracy of numerical solvers, model reso-
 388 lution) and emulator uncertainty. History matching rejects parameter values that
 389 lead to unacceptable model behavior (too large distance from the reference) and
 390 thus defines a not-ruled out yet (NROY) space, the model parameter space that
 391 cannot be further reduced given the sources of uncertainty.
- 392 • **6. Iterative refocusing** To reduce the emulator uncertainty, but only where needed,
 393 new iterations (or waves) following steps 3 to 5 are performed, sampling the NROY
 394 space obtained at the end of the previous wave for the design and only construct-
 395 ing emulators over the NROY domain.

396 Details on the different steps are given below. For simplicity, we first describe them for
 397 the first iteration and only one metric. Subsequent iterations and the addition of other
 398 metrics are discussed in Sect. 3.7. This section ends with a discussion about the rela-
 399 tionship between the present tool and more common tools used for calibration and sen-
 400 sitivity analysis.

401 **3.2 Step 1: Metric selection and references**

402 The metrics used to evaluate the SCM behavior depend on the physical situation
 403 considered and the parameterization hypothesis. Scalar metrics based on a dynamical
 404 or thermodynamical variable (e.g., potential temperature, water vapor mixing ratio, wind
 405 speed, cloud fraction) sampled at a given time can be used, such as the value at a given
 406 vertical level, the average or the maximum over a given layer (e.g., boundary layer, cloud
 407 layer), or the maximum over the whole atmospheric column. Radiation-oriented met-
 408 rics are particularly relevant to enhance the link between the present process-oriented
 409 model calibration and the calibration of the corresponding 3D configuration. Ideally, the
 410 chosen metric should be as insensitive as possible to the model vertical resolution. In that
 411 regard, integrals (or averages) are good candidates for scalar metrics, as will be illustrated
 412 in Part II. Root-mean square errors are not encouraged for two reasons, i/ there are usu-

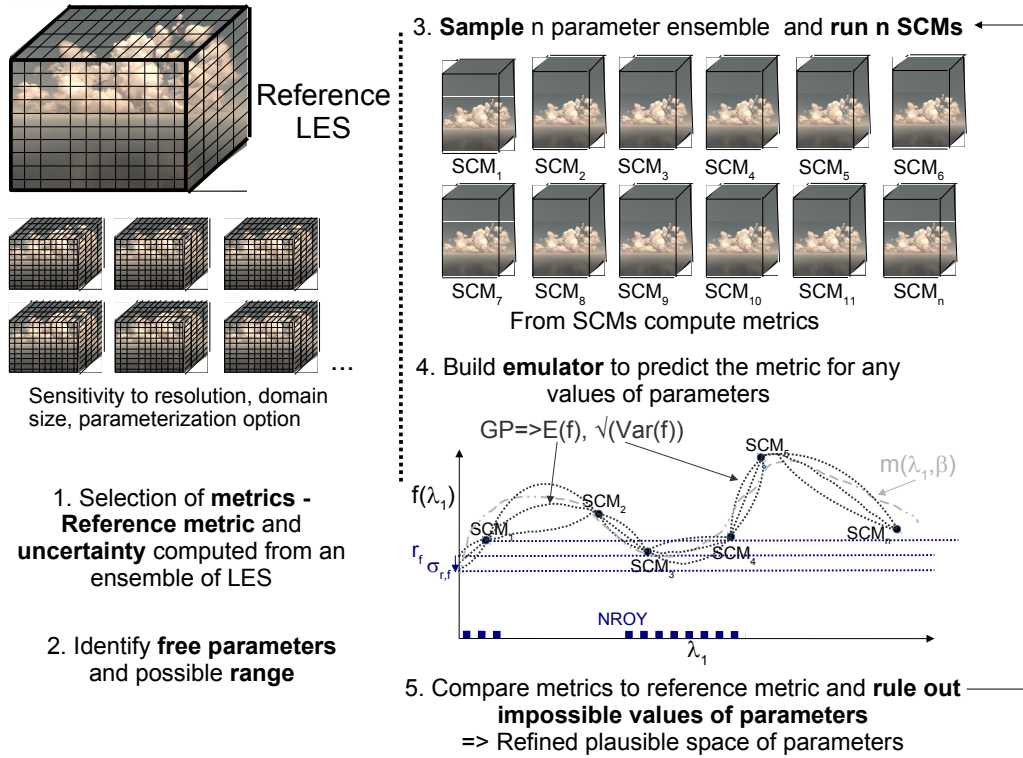


Figure 1. Schematic of the different steps of the htxplo tool

413 ally associated to a smaller signal to noise ratio and ii/ the Implausibility (see Sect. 3.6)
 414 is already a kind of root-mean square error. The number of metrics to be used is gen-
 415 erally of the order of ten, but it can be many more.

416 More complex metrics such as vertical profiles, time series or spatial fields, can also
 417 be considered. In that case, methods are used to reduce the dimensions of the outputs
 418 and principal component decomposition is one option (e.g., Salter et al., 2019). How-
 419 ever, scalar metrics, taken at a given time, or averaged over a short period of time, seem
 420 often sufficient to robustly constrain most of the SCM simulations (Personal communi-
 421 cation O Audouin). Therefore, in the present paper and in Part II, only scalar metrics
 422 will be used. They include boundary-layer average potential temperature and maximum
 423 cloud fraction.

424 References and their associated uncertainty are estimated from an LES ensemble.
 425 There are a priori two possibilities to build such an ensemble, which can be combined.
 426 The first consists in building the ensemble from simulations performed by different large-

427 eddy models, as has been done in several GCSS intercomparison exercises (Brown et al.,
428 2002; Siebesma et al., 2003; vanZanten et al., 2011; Pressel et al., 2017). The reference
429 thus corresponds to the LES ensemble mean, while the uncertainty is quantified by the
430 LES ensemble variance. The second option, used in this paper, relies on only one large-
431 eddy model and estimates the uncertainty around the reference model configuration by
432 performing sensitivity experiments to horizontal and vertical resolution, domain size, and
433 parameterization options (e.g., turbulence, microphysics, surface fluxes, radiation). In
434 this study, we have chosen to use the simulation realized with the higher resolution over
435 the largest domain and with the most relevant parameterization options as the reference,
436 but the ensemble mean could also be used. The large-eddy model used in this study is
437 the LES-configuration of Meso-NH (Lac et al., 2018). It makes use of a fourth-order cen-
438 tered discretization associated with an explicit fourth-order Runge-Kutta time integra-
439 tion. Figure 2 illustrates the spread obtained from a Meso-NH LES ensemble exploring
440 the sensitivity to horizontal, vertical resolution, domain size and options in the turbu-
441 lence and cloud schemes for one given case, namely the ARM Cumulus case, which is
442 a golden case for the study of continental cumulus (Brown et al., 2002). Table A2 in the
443 Appendix describes in detail the different simulations used to estimate the uncertainty.
444 Consistently with the literature (Brown et al., 2002; Matheou et al., 2011; vanZanten et
445 al., 2011; Zhang et al., 2017), domain-average conserved thermodynamical quantities are
446 weakly sensitive to changes in resolution, domain size and parameterization choices while
447 the domain-average liquid water content and cloud fraction exhibit more spread. Met-
448 rics derived from those latter quantities will therefore be associated to a larger uncer-
449 tainty. Figure 2 also indicates in grey shading the spread obtained from the LES inter-
450 comparison of Brown et al. (2002) highlighting a similar uncertainty estimate between
451 the two methods mentioned above. Similar results are obtained for LES ensembles of other
452 intercomparison exercises (not shown). For a given metric f , r_f is the reference metric
453 value, estimated from the reference LES simulation or the average of the LES ensem-
454 ble and $\sigma_{r,f}^2$ is the associated square error estimated from the LES ensemble. Note that,
455 in the absence of available LES, observations can also be used as a reference to be com-
456 pared to the SCM runs as illustrated in Ahmat Younous et al. (2018) but the observa-
457 tion error needs to be quantified.

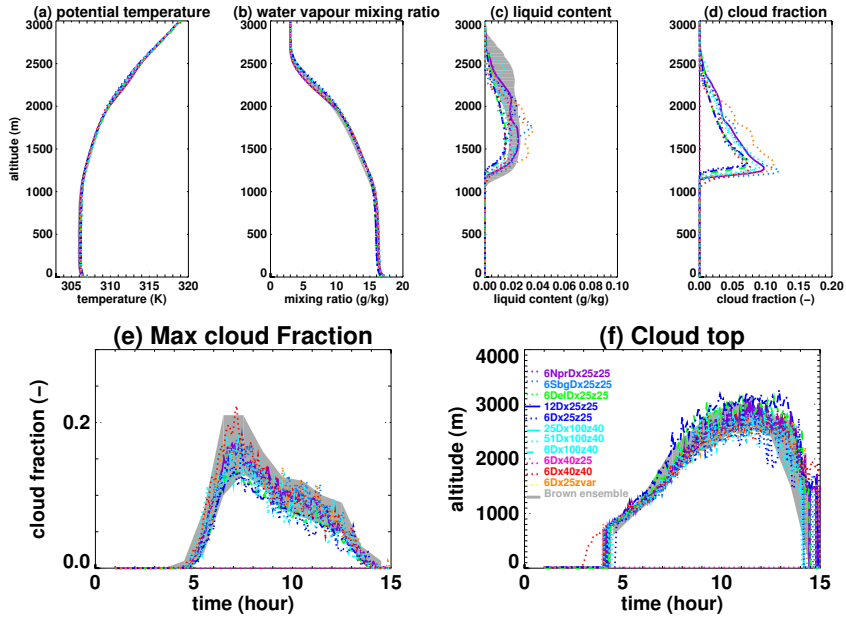


Figure 2. Vertical profile of (a) potential temperature, (b) water vapour mixing ratio, (c) liquid water content and (d) cloud fraction averaged over the horizontal domain at the 10th hour of the simulation (1530 LT) and time series of (f) the cloud top and (e) the maximum cloud fraction over the atmospheric column. The grey shading corresponds to the results of the Brown et al. (2002) intercomparison. The different color lines correspond to different sensitivity tests realized with Meso-NH changing either, one by one, the size of the domain, the vertical or horizontal resolution and some option in the cloud scheme, microphysics scheme or turbulence scheme (detailed in Table A2).

458 **3.3 Step 2: Selection of model parameters**

459 The number of model parameters can be large (generally on the order of 10 for each
 460 parameterization). Estimating the prior range of values that needs to be explored for
 461 each of them requires the modeler’s expertise and experience about the model and pa-
 462 rameterizations. The definition of this range is an important step as the results are only
 463 valid in this predefined parameter space (Williamson et al., 2013). So, we advise to choose
 464 a range as wide as possible in the absence of physical reasons or numerical concerns for
 465 constraining it. Nevertheless, the user might consider some tradeoff as the smaller the
 466 ranges, the smaller the space to explore.

467 As the tool samples any parameter independently from the others (see Step 3), the
 468 method remains efficient even though a parameter with no influence on the results was
 469 included. A sensitivity analysis (Oakley & O’Hagan, 2004) could be used as a prelim-
 470 inary step in order to reduce the number of parameters selected but may not be a good
 471 idea in general (see Sect. 3.8). Depending on the predefined range of parameter values,
 472 the user can consider either linear or logarithmic variations of the parameter values.

473 In the following, we consider a set of parameters $\boldsymbol{\lambda} = (\lambda_k)_k$, which is a subset of
 474 the model parameters $(\boldsymbol{\lambda}_p)_p$ (see Sect. 1).

475 **3.4 Step 3: Experimental design and SCM runs**

476 Once the model parameters are selected and their range of values defined, an ex-
 477 perimental design is built. It corresponds to the selection of a relatively small set of val-
 478 ues for the model parameters $(\boldsymbol{\lambda}_i)_{i=1,\dots,n}$, usually on the order of ten times the number
 479 of parameters. It explores the initial (or input) space of the parameter values in the range
 480 given for each parameter. An SCM simulation is performed for each of them and pro-
 481 vides the state vector $\boldsymbol{x}_c(\boldsymbol{\lambda}_i)$. The objective is to ”fill” the parameter space as uniformly
 482 as possible maximizing the minimum distance between points. Here, as classically used
 483 for the design of computer experiments, a Latin Hypercube (LHC) (Williamson et al.,
 484 2015) is used to efficiently sample the input parameter space. Classically, a LHC for a
 485 n-member ensemble uniformly divides each dimension of the input space into n bins that
 486 are sampled once each and only once. All the parameters are thus varied simultaneously
 487 in contrast to other sensitivity analysis approaches such as in the Morris sensitivity anal-

488 ysis (Saltelli, 2002), where parameters are varied one by one. The LHC sampling used
 489 here maximizes the minimum distance between the selected points of the input space.

490 More precisely, here we use k -extended latin hypercubes as proposed by Williamson
 491 (2015). It consists in producing several LHCs, added sequentially, which ensure that each
 492 additional LHC samples an area of the space that has not been sampled yet by the pre-
 493 vious LHCs. Such a design provides the advantage of being able to robustly check the
 494 GP performance on well-designed sub-LHCs.

495 **3.5 Step 4: Building emulators**

496 The selected metric (see Step 1) is computed for each SCM simulation, noted $f(\boldsymbol{\lambda}_i)$
 497 for $i = 1, \dots, n$. These numbers serve as a training dataset for the building of an em-
 498 ulator. The emulator is then used to predict the metric values $f(\boldsymbol{\lambda})$ for any vector of pa-
 499 rameter values $\boldsymbol{\lambda}$ in the input space.

Specifically, we use a Gaussian process (GP), a well known statistical model which
 has the advantage of interpolating observed model runs and provides a probabilistic pre-
 diction. The emulator gives a probability distribution for f written as:

$$f(\boldsymbol{\lambda}) \mid \boldsymbol{\beta}, \sigma^2, \boldsymbol{\delta} \sim \text{GP} \left(m(\boldsymbol{\lambda}, \boldsymbol{\beta}), k(\cdot, \cdot, \sigma^2, \boldsymbol{\delta}) \right),$$

where $m(\boldsymbol{\lambda}, \boldsymbol{\beta})$ is a prior mean function with parameters $\boldsymbol{\beta} = (\beta_i)_i$ and k a specified
 kernel (a covariance function describing the covariance between any 2 points). The ker-
 nel has a parameter that normally controls variance, σ^2 , and parameters δ_k for each di-
 mension of the input parameter λ_k that control the correlation attributed to each input.
 To start with, we assume a stationary kernel, i.e., the covariance only depends on the
 distance between points and not the absolute position. The GP is such that any finite
 collection $f(\boldsymbol{\lambda}_1), \dots, f(\boldsymbol{\lambda}_n)$ has a multivariate normal distribution with mean vector $m(\boldsymbol{\lambda}_1, \boldsymbol{\beta}), \dots, m(\boldsymbol{\lambda}_n, \boldsymbol{\beta})$,
 and variance matrix $\boldsymbol{\Sigma}$ with $\Sigma_{ij} = k(\boldsymbol{\lambda}_i, \boldsymbol{\lambda}_j, \sigma^2, \boldsymbol{\delta})$. Let the training data be $\mathbf{F} = (f(\boldsymbol{\lambda}_i))_{i=1, \dots, n}$,
 then

$$f(\boldsymbol{\lambda}) \mid \mathbf{F}, \boldsymbol{\beta}, \sigma^2, \boldsymbol{\delta} \sim \text{GP} \left(m^*(\boldsymbol{\lambda}, \boldsymbol{\beta}), k^*(\cdot, \cdot, \sigma^2, \boldsymbol{\delta}) \right),$$

500 where there are well-known closed form expressions for m^* and k^* (Williamson et al.,
 501 2017). Note that m^* and k^* are the updated mean and covariance representing what the
 502 emulator has ‘learned’ from the data, \mathbf{F} .

503 Whilst there are many possible prior choices of m and k , htexplo uses a 2-phase
 504 approach. First, we impose a structured mean surface $m(\boldsymbol{\lambda}, \boldsymbol{\beta}) = \boldsymbol{\beta}^T \boldsymbol{g}(\boldsymbol{\lambda})$ as a linear
 505 combination of simple functions of the input parameters contained in the vector $\boldsymbol{g}(\boldsymbol{\lambda})$
 506 (e.g. monomials, Fourier functions and interaction terms are chosen through the forwards
 507 selection and backwards elimination method described in Williamson et al. (2013)). In
 508 the second stage, we use the squared exponential kernel function and Hamiltonian Monte
 509 Carlo (HMC, implemented in Stan – Carpenter & Coauthors, 2017) to sample from the
 510 posterior distribution of the parameters $\boldsymbol{\beta}$, σ^2 , and $\boldsymbol{\delta}$ given \boldsymbol{F} (note that the mean sur-
 511 face $m(\boldsymbol{\lambda}, \boldsymbol{\beta})$ is not directly fitted in phase 1, but its structure is chosen, with Bayesian
 512 inference ultimately used in fitting for phase 2).

513 The choice of HMC implemented in Stan was motivated by requiring robust au-
 514 tomation of emulator building across many metrics and cases, without needing the con-
 515 stant statistical expertise to diagnose MCMC convergence issues and to fix them by hand
 516 each time. Stan affords us with the ability to specify flexible and intuitive priors, and
 517 we use weakly informative priors as advocated by Gelman (2006). With the exception
 518 of the intercept term (which is uniform), our prior for each $\boldsymbol{\beta}$ is $N(0, 10)$ and we use the
 519 OLS fitted values as starting values for the HMC. We set $\delta_k \sim \text{Gamma}(4, 4)$ for all k
 520 to allow a wide range of potential correlation structures (this is a weakly informative prior)
 521 whilst penalising very small values that typically have high likelihoods, but lead to em-
 522 ulators with no predictive power (for discussion, see Volodina, 2020). Our prior for σ^2
 523 is a truncated Normal (at 0), with mean at the residual from our OLS fits, and variance
 524 set using the variability of the ensemble (full details for these choices in Volodina, 2020).

525 The emulator is then tested using standardized Leave One Out diagnostics on the
 526 training data. These tests remove one point at a time from the training set and use
 527 the emulator fitted on the remaining data to predict the removed point. Repeated over
 528 the training set, we then check whether the majority of left out points lie within 95%
 529 prediction intervals (we would expect 5% to miss). We also remove sub-designs from the
 530 training set and attempt to predict the whole sub-design, again checking to see if we have
 531 good posterior coverage of the ensemble. If the emulator fails these checks we revisit the
 532 computation of the emulator. For example, the procedure described in Volodina and Williamson
 533 (2020) (and available in htexplo) can be used to derive an appropriate non-stationary
 534 kernel k before refitting the emulator by HMC. Once fitted, the GP expectation $E[f(\boldsymbol{\lambda})]$

535 provides an estimation of the metric for any given $\boldsymbol{\lambda}$, and its variance $\text{Var}[f(\boldsymbol{\lambda})]$ provides
 536 an uncertainty around this estimation.

537 SCM runs are computationally cheap, but the fitted emulators are even cheaper
 538 and thus allow the computation of millions of predictions, with associated uncertainties,
 539 in a short time (a few minutes). This enables us to numerically define the space contain-
 540 ing acceptable sets of parameters with respect to the chosen metrics and in particular,
 541 to visualize it (Step 5). The choice of Stan has proven effective for this project, though
 542 it does not scale well to larger ensembles. Going forward, a new version of the tools de-
 543 faulting to MAP estimation and using efficient parallel implementation has just been re-
 544 leased enabling millions of predictions in just a few seconds (Williamson & Volodina, 2020).

545 **3.6 Step 5: History matching**

The htxplo tool relies on the history matching technique, which seeks to rule out
 parameter values from the input space that are “implausible”, given the SCM behav-
 ior for these parameter values and the sources of uncertainty. These sources include the
 reference (observation) error, treated as a random quantity with mean 0 and variance
 $\sigma_{r,f}^2$, and the SCM discrepancy, which has mean 0 (unless the user knows the direction
 in which the model is biased) and variance $\sigma_{d,f}^2$ (Sexton et al., 2011). The emulator is
 used to estimate the model behavior on a much larger sample of the input space than
 possible with the SCM. To history match the SCM behavior, we introduce the “Implau-
 sibility” measure for the metric f (Williamson et al., 2013), $I_f(\boldsymbol{\lambda})$, which is a distance
 between the metric prediction $f(\boldsymbol{\lambda})$ by the emulator at $\boldsymbol{\lambda}$, and the reference metric value,
 r_f , with respect to the norm induced by our second-order uncertainty specification, noted
 $\|\cdot\|_H$ below. The Implausibility reads

$$\begin{aligned} I_f(\boldsymbol{\lambda}) = \|r_f - f(\boldsymbol{\lambda})\|_H &= \frac{|r_f - \text{E}[f(\boldsymbol{\lambda})]|}{\sqrt{\text{Var}[r_f - \text{E}[f(\boldsymbol{\lambda})]]}} \\ &= \frac{|r_f - \text{E}[f(\boldsymbol{\lambda})]|}{\sqrt{\sigma_{r,f}^2 + \sigma_{d,f}^2 + \text{Var}[f(\boldsymbol{\lambda})]}}. \end{aligned} \quad (5)$$

546 The model discrepancy for the metric f , $\sigma_{d,f}$, accounts for the model structural
 547 error due to the inherent inability of the SCM to reproduce the LES exactly (due to un-
 548 resolved physics or missing processes, for example). It could be defined as the minimum
 549 error possible when exploring the full set of parameters, however, this could permit the
 550 SCM to be close to the reference for the wrong reasons and does not account for mul-

551 multiple metrics and cases, so we avoid this definition. Instead it is typically defined to be
 552 the uncertainty left in the difference between the SCM metric when the parameters are
 553 fixed at their best values (fixed the same for all metrics) and the references. This quan-
 554 tity is perhaps the target of model development in the first place and, as such, is unknown.
 555 For example, suppose we want to test the ability of a new parameterization to capture
 556 the behaviour of the reference. With the standard definition of discrepancy, the uncer-
 557 tainty needed so that the new parameterization captures the behaviour of the reference,
 558 it is not clear how to proceed with testing. Our approach instead is to treat model dis-
 559 crepancy as a “tolerance to error” as detailed in Williamson et al. (2017). The tolerance
 560 to error is the distance between model results and the reference that the modeler would
 561 be satisfied with, enabling modellers to place confidence in certain metrics/parts of their
 562 parameterization, and relax restrictions on others as needed. As illustrated in Sect. 4
 563 and Part II, defining this tolerance to error can be a difficult a-priori task; however ex-
 564 perimenting with this value provides important insights into the behavior and its inher-
 565 ent limitations. The most attractive feature of this approach to discrepancy is that, for
 566 a given tolerance to error, if the induced NROY space is empty it means that the pa-
 567 rameterization is not able to reproduce the reference under the given tolerance. Either
 568 the tolerance can be relaxed, accepting the limitations of the current set of parameter-
 569 izations, or the parameterization can be revisited.

The implausibility defines a membership rule for NROY space after the first iter-
 ation:

$$\text{NROY}_f^1 = \{\boldsymbol{\lambda} \mid I_f(\boldsymbol{\lambda}) < T\}.$$

570 where T is a chosen threshold (or cutoff). For scalar metrics, it is standard to use $T =$
 571 3 justified using Pukelsheim’s rule that states 95% of the probability density for any uni-
 572 modal distribution is within 3 standard deviations of the mean (Pukelsheim, 1994). Us-
 573 ing this threshold makes it unlikely that good parameter values are ruled out by chance.
 574 To measure and visualize NROY space the Implausibility $I_f(\boldsymbol{\lambda})$ is calculated on a ran-
 575 dom LHC sampling of a large number (on the order of hundreds of thousands or millions)
 576 of vectors $\boldsymbol{\lambda}$.

577 Note that $I_f(\boldsymbol{\lambda})$ can be smaller than the chosen threshold T either because $E[f(\boldsymbol{\lambda})]$
 578 is close to the reference or because the sum of the different errors is large. When the un-
 579 certainty of the emulator is larger than the tolerance to error and observation error, points

580 that should be ruled out are kept in the NROY. In this case, further iterations are de-
 581 sirable in order to increase the density of the sampling of NROY and hence improve the
 582 emulator quality and reduce the associated uncertainty.

583 **3.7 Iterative refocusing and multi-metrics**

584 One advantage of this method is to progressively optimize the design of simulations
 585 to be run. New simulations are iteratively added only where it is useful to increase the
 586 emulator accuracy. This is performed by iterating the same process previously described
 587 several times in "waves", (this is termed "iterative refocusing" and is a fundamental part
 588 of the history matching approach). Each new iteration n starts from the remaining space
 589 NROY_f^{n-1} estimated at the end of the previous wave. Because of its complex geometry,
 590 a LHC sampling, as in the first wave, cannot be applied, and therefore the remaining space
 591 is re-sampled uniformly. A new SCM simulation ensemble is performed with this design
 592 and is used to proceed with steps 4 and 5. The new emulator is only valid in the new
 593 parameter space, namely NROY_f^{n-1} . Outside this space, we rely on the emulators from
 594 the previous waves. As in Step 5, to measure and visualize NROY_f^n , the implausibility
 595 is computed over a large number of points in the input space. The threshold T may be
 596 varied between waves, but we advise to keep it to 3 as long as the process has not con-
 597 verged (i.e. the emulator variance within the current NROY space remains large – see
 598 also Sect. 4 and Part II). The iterative refocusing stops when the convergence of the se-
 599 quence $(\text{NROY}_f^n)_n$ has been qualitatively achieved.

So far, we have considered only one metric, but several metrics $(f_k)_k$ can be com-
 bined at the same time. An Implausibility is then computed for each metric and the to-
 tal NROY^n space is the intersection of the $\text{NROY}_{f_k}^n$ associated with each metric:

$$\text{NROY}^n = \bigcap_k \text{NROY}_{f_k}^n = \{ \boldsymbol{\lambda} \mid \#\{k \mid I_{f_k}^n(\boldsymbol{\lambda}) > T\} \leq \tau \},$$

600 # represents the number of metrics fulfilling the condition indicated into brackets (where
 601 the implausibility is greater than the threshold) and τ , the number of metrics for which
 602 the model is allowed to be far from the reference while still kept in the NROY space. If
 603 $\tau = 0$, all metrics must satisfy our implausibility cutoff. If there are a large number of
 604 metrics then τ should be increased ($\tau \geq 1$) to avoid multiple testing problems mean-
 605 ing that too many good parameter values are ruled out by chance. If a modeller seeks
 606 to prioritize certain metrics, they can either be introduced in early waves, ensuring that

607 the NROY space satisfies priority metrics first before introducing new ones, or the tol-
608 erance to error, which is defined for each metric, can be used to impose priorities (a larger
609 tolerance to error induces a less constraining metric).

610 **3.8 Sensitivity analysis provided by the tool**

611 The htexplo tool provides its own sensitivity analysis, which, due to the use of multi-
612 wave history matching, is rather different from traditional methods applied to models
613 throughout the literature. Traditional methods, either derivative-based (Saltelli, 2002),
614 or variation-based (Oakley & O’Hagan, 2004), essentially seek to identify which param-
615 eters modify model output. This can help focus further study, model development or even
616 observation collection to help understand these parameters. Note that the htexplo tool
617 provides at the first iteration a sensitivity analysis over the entire space where correla-
618 tion among parameters is included as the parameters are not varied one at a time.

619 However, for calibration purposes, once history matching is considered as a valid
620 approach for a given model, the sensitivity analysis should not be done on the full model
621 input space. By using history matching, we acknowledge that there is a large part of the
622 model parameter space that is not useful for understanding reality. The Gaussian pro-
623 cesses remove this uninformative space in order to target the space where the model be-
624 comes useful. Once we have this useful subspace, the usual and important questions that
625 are posed by sensitivity analysis should be considered. For example, how is the model
626 output changing as we move through parameter space and which parameters are respon-
627 sible for these changes? As all models within the NROY space are consistent with our
628 metrics, sensitivity analysis as described here is now really focused on the relevant sub-
629 space. Note that sensitivity analysis on the original input space does not answer these
630 questions. Seen through the history matching lens, on the full space, sensitivity anal-
631 ysis is showing us which parameters are responsible for the variability in the space we
632 are about to cut. Whilst informative for helping us cut the space efficiently, sensitivity
633 analysis is not necessary at this stage. Our methods are already efficiently able to do this.

634 Performing variance-based sensitivity analysis in NROY space is not trivial and we
635 are not aware of any methods that are currently able to do this. Variance-based sensi-
636 tivity analysis requires independent input spaces (which is what we always start with
637 in wave 1). But after cutting space, we have complex relationships between the param-

638 eters. NROY space may not even be simply connected, and can be highly non-linear. Ef-
639 ficient methods for calculating sensitivity in these unusual spaces would be interesting
640 to apply for history matching as an avenue for further research.

641 As a practical tool, the density plots such as those given in Fig. 5, provide their
642 own type of second-order sensitivity analysis. They allow us to see, as we move in two
643 dimensions of a parameter space, how the shape is changing and, moreover, which com-
644 binations of parameters it is important to get right and, not usually included in a sen-
645 sitivity analysis, how they need to be set in order to get sensible answers. As well as all
646 of the benefits we have for tuning, we would argue that history matching is achieving
647 many of the same things that a sensitivity analysis achieves in terms of informing the
648 modelling, but concentrated only on the model input space that is consistent with the
649 observations.

650 **3.9 On the use of history matching and the avoidance of optimization**

651 Whilst History matching is well established and is being used in a growing num-
652 ber of climate studies, other methods of calibration are more popular and we believe should
653 be avoided for process-based model development. Whilst many methods based on op-
654 timizing a cost function exist (Hourdin et al., 2017), the most popular in the UQ com-
655 munity is Bayesian calibration (Kennedy & O’Hagan, 2001). Bayesian calibration requires
656 a similar set up to history matching (emulators, observation errors and model discrep-
657 ancy) and then jointly finds the posterior probability distribution of the “best” value of
658 the input parameters and the model discrepancy (strong prior information on the dis-
659 crepancy is required to make this sensible, Brynjarsdóttir & O’Hagan, 2014). Optimiza-
660 tion methods like these do not afford us with the chance to falsify a parameterization
661 (they always find the best value), nor do they give all parameter values that are consis-
662 tent with the observations (in our case reference LES) that can then be used when tun-
663 ing the 3D model (see Part II).

664 **4 Illustration of htexplo on a simple case**

665 In this section, the use of htexplo is illustrated for the ARPEGE-Climat 6.3 atmo-
666 spheric model based on a single 1D case. More comprehensive exploitation of the tool
667 will be given in Part II.

668 **4.1 Model, parameters and case-study**

669 ARPEGE-Climat 6.3 is the atmospheric component of the CNRM-CM6-1 climate
 670 model (Voltaire et al., 2019; Roehrig et al., 2020). It has 91 vertical levels, 15 of them
 671 below 1500 m. The model time step is 15 minutes. Here, we use its SCM version and
 672 focus on its representation of a clear convective boundary layer. To simulate the processes
 673 involved in the boundary layer, the model combines a turbulence scheme with a mass-
 674 flux scheme, thus following the Eddy-Diffusivity Mass-Flux framework (e.g. Hourdin
 675 et al., 2002; Soares et al., 2004; Siebesma et al., 2007; Pergaud et al., 2009). The mass-
 676 flux scheme represents convection in a unified way from the clear convective boundary
 677 layer regime to the shallow cumulus and deep convection regimes (Piriou et al., 2007;
 678 Gueremy, 2011). In this section, we aim at analyzing the importance of the values of free
 679 parameters of the turbulence scheme on the simulation of an idealized clear boundary
 680 layer. A boundary-layer-top vertical entrainment is activated in the default version of
 681 ARPEGE-Climat 6.3 (see (Roehrig et al., 2020)). For the sake of simplicity of the present
 682 illustration, and also because this parameterization is weakly active in the analyzed case,
 683 it is fully deactivated in the following section. Similar results are obtained when it is ac-
 684 tivated.

The turbulence scheme is based on Cuxart et al. (2000) which aims at providing the vertical turbulent fluxes from which the turbulent source term is derived for the prognostic variables (see more details in Roehrig et al., 2020). The scheme relies on a prognostic equation of the grid-scale turbulence kinetic energy, \bar{e} :

$$\frac{\partial e}{\partial t} = \frac{-1}{\rho} \frac{\partial(\overline{\rho w' e'})}{\partial z} - (\overline{w' u'} \frac{\partial \bar{u}}{\partial z} + \overline{w' v'} \frac{\partial \bar{v}}{\partial z}) + \beta \overline{w' \theta'_{vl}} - \frac{\bar{e}^{3/2}}{L_\epsilon} \quad (6)$$

where the advection terms, the pressure fluctuations and the diffusion transport have been neglected. ρ is the air density, w the vertical velocity, u and v the zonal and meridional wind components, β is the buoyancy parameter (equal to $\frac{g}{\theta}$ with g the gravitational constant, θ being the potential temperature), θ_{vl} is the liquid virtual potential temperature and L_ϵ the dissipation length. Primes indicate fluctuations with respect to the grid-scale values indicated with overbars. The different turbulent vertical fluxes are diagnosed using \bar{e} following, for any variable φ :

$$\overline{w' \varphi'}(z) = -K_\varphi \frac{\partial \bar{\varphi}(z)}{\partial z} \quad (7)$$

with

$$K_\varphi = \sqrt{\bar{e}} L_m A_\varphi \Phi_\varphi \quad (8)$$

685 with Φ_φ a stability function also computed at each altitude (for more details see Cuxart
686 et al. (2000)) and A_φ a free parameter. The mixing length, L_m , is computed following
687 Bougeault and Lacarrere (1989); it consists in computing the vertical displacement an
688 air parcel can travel upwards and downwards with its available turbulence kinetic en-
689 ergy according to the thermal stratification. Also, L_ϵ in Eq. 6 is defined by $L_\epsilon = A_\epsilon \times$
690 L_m with A_ϵ another free parameter. Finally, we have selected three parameters for this
691 analysis namely, A_ϵ controlling the expression of the dissipation length-scale as a func-
692 tion of the mixing length-scale and A_U and A_T that respectively enter into the expres-
693 sion of the exchange coefficient in Eq. 8 for the wind and the temperature (the same co-
694 efficient, A_U , is used for both the zonal and meridional component of the wind). The range
695 of variation explored for each parameter is indicated in Table 1 and the parameters are
696 varied linearly in those ranges (when parameter ranges span many orders of magnitude,
697 we typically vary them on a log scale and htxplo is set up to do this). The turbulence
698 parameterization includes other free parameters but to keep the example simple, the three
699 most influential parameters for this case have been selected and no free parameters of
700 the mass-flux scheme are considered.

Table 1. List of the free parameters of the turbulence scheme that are varied in this example with default values and range of variation

Names	A_U	A_ϵ	A_T
Default	0.126	0.85	0.14
Minimum	0.01	0.1	0.01
Maximum	0.4	3.	1.

701 To keep the example simple, only one case is used here. This case is a dry ideal-
702 ized case of a convective boundary layer with a constant-in-time large surface sensible
703 heat flux of 0.24 Kms^{-1} with a strongly capped boundary layer documented in Ayotte
704 et al. (1996), called 24SC in the following. The importance of combining different cases
705 will be illustrated in part II.

706 We first document a sequence of three waves where additional metrics are added
707 at each iteration (Experiment 1). We will then discuss the results obtained when adding
708 all the metrics directly at wave 1 (Experiment 2), varying the threshold used to deter-

709 mine the NROY (Experiment 3 see also Sect. 3.5), using more SCM runs (Experiment
710 4), and varying the tolerance to error (Experiments 5 and 6).

711 4.2 Three consecutive waves adding metrics progressively

712 For the first iteration (or wave in the following) of Experiment 1, 30 SCM simu-
713 lations of the 24SC case were realized by varying values for the three parameters explor-
714 ing at best (using a LHC sampling, see Sect. 3.4) the range of each parameters (Table 1).
715 Figure 3 illustrates that the parameters are randomly sampled as indicated by the dis-
716 tribution of the black dots along the different x-axes. Three different metrics are used
717 to characterize the turbulent mixing in the boundary layer and are progressively intro-
718 duced through the successive waves. The first chosen metric is the potential tempera-
719 ture averaged over the layer 400-600 m. It is a good proxy for the boundary-layer po-
720 tential temperature, which is well mixed between the surface and the boundary-layer top,
721 located around 1300 m. This metric is computed for the 30 SCM runs; these computa-
722 tions serve as training data for the construction of the emulator. The prior mean func-
723 tion (see Sect. 3.5), m for this emulator is a sum of linear and quadratic functions of the
724 parameters. The stationary squared-exponential kernel provides a sufficient fit to the data
725 according to the leave-one-out methodology explained in Sect. 3.5. Figure 3 presents the
726 variation of the metric as a function of the parameters: some first-order relationships ap-
727 pear with the boundary-layer potential temperature increasing with A_U and A_T to a lesser
728 extent A_T (due to an increased mixing associated to a larger diffusivity and larger fluxes)
729 and decreasing with A_ϵ (due to a reduced mixing because of the increased dissipation).
730 For this metric, we have chosen a tolerance to error of 0.5 K, a difference between SCM
731 results and LES we are satisfied with. This may be a bit large for this very idealized case
732 (with no moisture, an already convective initial state) but this is an error we will be sat-
733 isfied with generally for boundary-layer potential temperature. Given this tolerance to
734 error (indicated by the dashed horizontal grey line), the metric does not provide much
735 constraint on the model behavior and the entire initial parameter space is kept (c.f. Ta-
736 ble 2). Note that this tolerance to error is much larger than the uncertainty around the
737 LES ($\sigma_{r,f} = 0.075$ K) and the emulator ($\text{Var}[f(\boldsymbol{\lambda})] = 0.042$ K). Sect. 4.3 details the
738 effect of a reduced tolerance to error.

A second wave is realized, with 30 runs sampling the NROY space of the first wave
(the previous 30 SCM runs could also have been used for efficiency), which is in fact the

Table 2. Description of the model discrepancy (Disc.) of the given metric (indicated in the 2nd, 3rd and 4th columns), the Cutoff, threshold used for Implausibility (5th column), the Not-Ruled-out-Yet Space (fraction in % of initial space of parameters, 6th column) and the emulator uncertainty quantified as the emulator standard deviation for each metric (7th column) for each Experiment and wave.

N° Expt N° Wave	Disc. θ_{BL} [K]	Disc. Ay_{θ} [Kms ⁻¹]	Disc. ws_{BL} [m s ⁻¹]	Cutoff	NROY= % of initial space	Emulator Error for θ_{BL} / Ay_{θ} / ws_{BL}
Exp1-1	0.5	-	-	3	100	0.042/-/-
Exp1-2	0.5	0.05	-	3	30	0.022/0.014/-
Exp1-3	0.5	0.05	1	3	23	0.069/0.023/0.049
Exp2-1	0.5	0.05	1	3	40	0.042/0.019/0.22
Exp2-2	0.5	0.05	1	3	38	0.033/0.017/0.06
Exp2-3	0.5	0.05	1	3	27	0.13/0.036/0.14
Exp3-1	0.5	0.05	1	3	72	0.022/0.063/0.019
Exp3-2	0.5	0.05	1	3	32	0.060/0.021/0.15
Exp3-3	0.5	0.05	1	2.5	22	0.092/0.026/0.054
Exp3-4	0.5	0.05	1	2.	15	0.076/0.019/0.061
Exp4-1	0.5	0.05	1	3	27	0.038/0.013/0.033
Exp5-1	0.25	0.025	0.5	3	32	0.043/0.020/0.21
Exp6-1	0.1	0.01	0.25	3	31	0.041/0.020/0.21

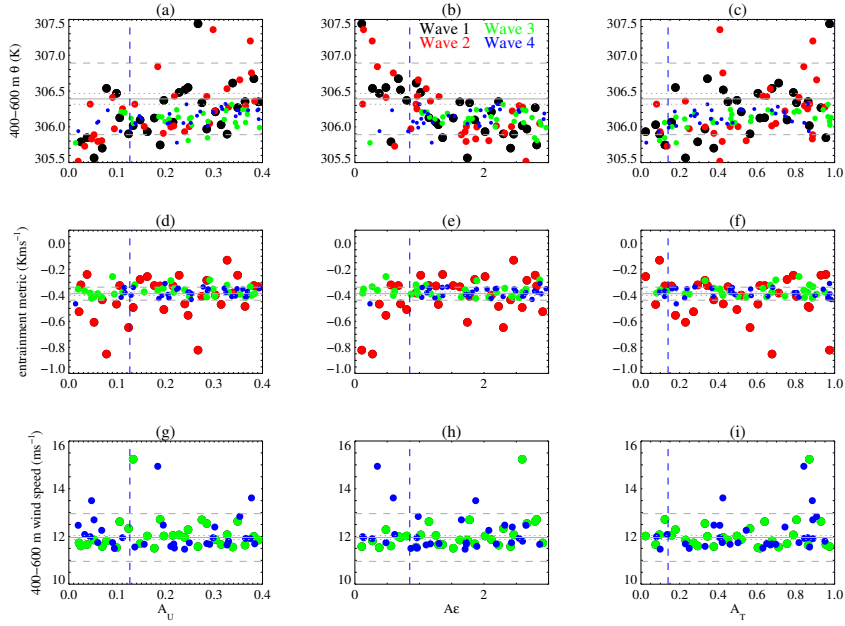


Figure 3. The three metrics, boundary-layer potential temperature (a–c), entrainment metric (d–f) and boundary-layer windspeed (g–i) are plotted as a function of the value of each parameter, A_U (a, d, g), A_ϵ (b, e, h) and A_T (c, f, i). A different color is used for the different waves of Experiment 1 (black for Wave 1, red for Wave 2, green for Wave 3 and blue for Wave 4). The vertical dashed blue line corresponds to the default value of the parameter used in the model, the horizontal thin full grey line correspond to the reference metric and the dotted lines indicates the uncertainty around this reference from the different LES simulations while the dashed lines indicate the tolerance to error around the reference.

entire initial parameter space as the first metric did not constrain the parameter space. Two metrics are computed from those 30 runs: the potential temperature averaged between 400 m and 600 m as in the first wave and the entrainment metric, A , quantifying the overshoot of the boundary layer relative to the initial profile as defined in Ayotte et al. (1996). A is computed as:

$$A = \frac{\int_{zi(t_0)}^H (\theta(z, t_f) - \theta(z, t_0)) dz}{t_f - t_0} = \frac{\int_0^H (\max(\theta(z, t_f) - \theta(z, t_0), 0)) dz}{t_f - t_0}$$

739 t_0 being the initial time, t_f the time at which the metric is computed and H the top of
 740 the model or a level largely above the boundary-layer top. This metric is less commonly
 741 used for evaluating models and it was more difficult to specify a tolerance to error which
 742 was taken as 0.05 K.m s^{-1} . An emulator is built for each metric. The second metric is
 743 more restrictive and the NROY space is now reduced to 30% of the initial parameter space
 744 (Table 2). The obtained NROY (not shown) is not very different from the one obtained
 745 for the third wave. It excludes values of the parameters that lead to simulations with
 746 too large or too small entrainment metric as indicated by the differences between the red
 747 dots and the green ones in Fig. 3.

748 A third wave is realized, with 30 new SCM runs sampling the new NROY. Three
 749 metrics are computed from those 30 runs: the two previous ones plus the wind speed av-
 750 eraged between 400 m and 600 m. For this last metric, we fixed the tolerance to error
 751 to 1 m s^{-1} . After this third iteration, the NROY is 23% of the initial space. As shown
 752 in Fig. 4, the spread of the different simulations that sampled the parameter values re-
 753 duces progressively throughout the different waves and this tool allows to discard val-
 754 ues of parameters that induce a too deep boundary layer. The wind-speed profiles did
 755 not completely converge and this is associated to the observation uncertainty which has
 756 been fixed to 1 ms^{-1} .

757 The final NROY space after the third wave is shown in Fig. 5. The metrics tend
 758 to reject preferentially low values of A_ϵ with high values of A_U or high values of A_ϵ with
 759 low values of A_U underlying some correlation between these two parameters. Note the
 760 default values of the parameters are within the NROY space confirming that they cor-
 761 respond to an acceptable calibration of the turbulence scheme, given the chosen toler-
 762 ance to error and the LES uncertainty. This is also confirmed by the simulations of the
 763 last wave having a behavior similar to the default simulation as shown in Fig. 4.

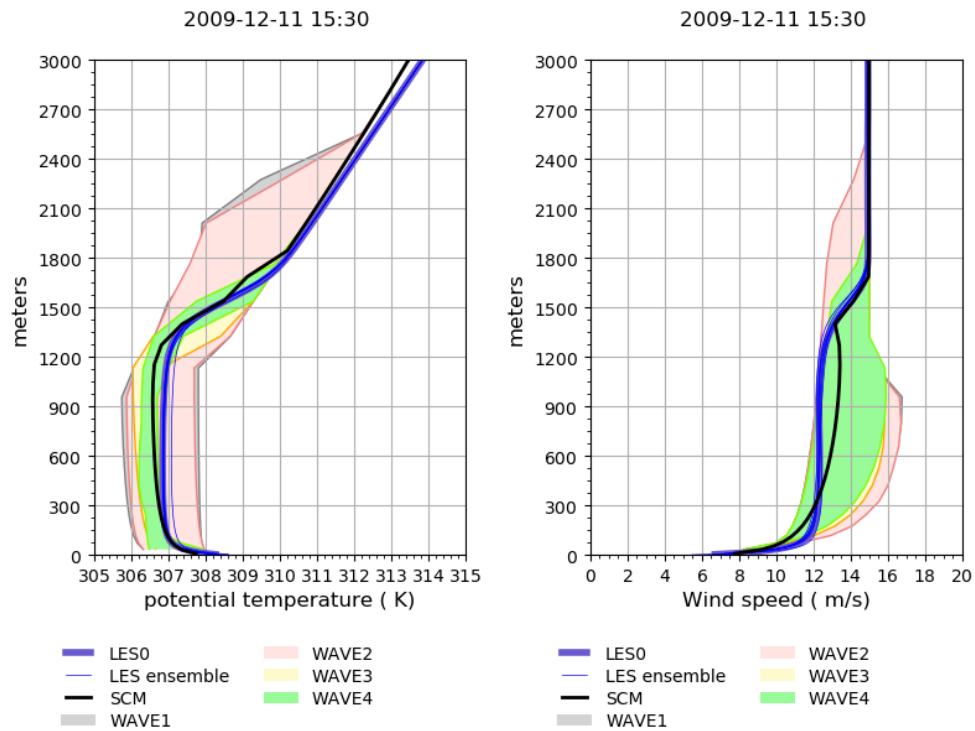


Figure 4. Vertical profile of (a) potential temperature and (b) wind speed for the last hour of the simulation with the spread of the ensemble of simulations used for the different waves indicated in different color shadings for Exp 1, the default simulation is in black, the reference LES in thick dark blue and the different elements of the LES ensemble in thin blue lines.

764 The uncertainty around the LES obtained from eight different LES runs with slightly
 765 different configurations, detailed in the appendix, is 0.075 K for θ_{BL} , 0.014 K m s^{-1} for
 766 A_θ and 0.083 m s^{-1} for ws_{BL} , on the same order of magnitude of the emulator uncer-
 767 tainty. For the first metric and third metric, the tolerance to error is much larger than
 768 the uncertainties of the reference and the emulator while for the second metric the three
 769 uncertainties are of the same order of magnitude. Concerning the tolerance errors, we
 770 can conclude that for this case and the selected metrics, the SCM is good enough for a
 771 sub-domain of the initial parameter space.

772 4.3 Robustness

773 In this subsection, we analyze the sensitivity of the results to i) the sequence of in-
 774 troduction of metrics (Experiment 2 uses the three metrics directly at wave 1), ii) the
 775 threshold used to determine the NROY space (Experiment 3), iii) the number of SCM
 776 runs used to form the training dataset (Experiment 4), and, iv) the tolerance to error
 777 (Experiments 5 and 6).

778 If the three metrics are introduced directly in the first wave (Experiment 2), the
 779 NROY space is similar to the one obtained after three waves (see Table 2 and Fig. 5)
 780 although the NROY space is larger (40% against 23%). Repeating more waves with the
 781 same metrics allows to progressively converge to the same NROY space. Note that a test
 782 with only one metric but the most constraining one, namely the entrainment metric, leads
 783 to very similar result ($NROY = 43\%$) for the first wave (not shown). Although not il-
 784 lustrated for this case, introducing one by one the metric, is sometimes important: i/
 785 it can allow to give some priority among the metrics, finding first a space consistent with
 786 the first metric in which the second metric is then used as a constraint and ii/ if one met-
 787 ric has a strong non-linear behaviour reducing the initial parameter spaces with other
 788 metrics may ease the capacity of the emulator to reproduce the metric behaviour. These
 789 results also indicate that adding a new metric in the core of the process does not alter
 790 the selection, allowing to add supplementary metrics if one realizes that some behavior
 791 of the SCM is not constrained enough, a fundamental aspect of history matching.

792 In Experiment 3, we first realize two waves as in Experiment 2 and then progres-
 793 sively reduce the threshold used to determine the NROY space from 3 to 2.5 in Wave
 794 3 and from 2.5 to 2 in Wave 4 (see Table 2) to explore the impact of less conservative

795 threshold (a threshold of 3 corresponds to ruling out what exceeds three times the un-
 796 certainties and keeps 95% of the probability for any unimodal probability distribution).
 797 The differences in the NROY space of the first wave with Exp2-1 indicates that 30 SCM
 798 runs are probably not enough to robustly constrain the first iteration and more itera-
 799 tions are needed. Then, reducing the cutoff induces a smaller NROY space but the change
 800 is not radical. This was expected from the lower left figures of Fig. 5 that show the min-
 801 imum value of the Implausibility for any variations of the other parameters (here, the
 802 third parameter). Indeed, the area with minimum value of $I_f(\boldsymbol{\lambda}) > 3$ (i.e. the points
 803 that are excluded from the NROY space whatever the value of the third parameter) is
 804 very similar to the area with minimum value of $I_f(\boldsymbol{\lambda}) > 2$.

805 All of the previous experiments have been realized using a rather small training dataset
 806 of 30 SCM runs (ten times the number of parameters). Experiment 4 has tested the im-
 807 pact of using 90 SCM runs instead of 30 for wave 1. This experiment produces directly
 808 a smaller NROY space (see Fig. 6) at the first wave than obtained from 30 SCM runs
 809 (see Exp3-1 or Exp2-1 in Table 2). Also, the emulator uncertainty is smaller for the first
 810 wave of Experiment 4 than the ones of the first wave of Experiment 2 or 3. A compro-
 811 mise must be found between a larger ensemble of simulations that increases robustness
 812 but is more costly.

813 The sensitivity to the tolerance to error is illustrated in Table 2 and Fig. 6 with
 814 Experiments 5 and 6. When reducing the tolerance to error by a factor of two the NROY
 815 space is 32% of the initial space in Exp5-1 (using the three metrics at once, so to be com-
 816 pared to 40%). The NROY space (31% of the initial space) is not much reduced further
 817 when reducing the tolerance to error twice more (Exp6-1), because the tolerance to er-
 818 ror is not anymore the limiting uncertainty. It is interesting to note that even when strongly
 819 reducing the tolerance to error, the default values for the three selected parameters are
 820 still in the NROY space validating the choice of parameter values used in the control sim-
 821 ulation. The lower left panel of the subfigures in Fig. 5 and Fig. 6 indicates the mini-
 822 mum Implausibility along the other dimensions of the space and as illustrated in Fig. 6,
 823 reducing the tolerance error (when larger than the other errors) induces a reduction of
 824 the denominator in the Implausibility and therefore an increase of Implausibility.

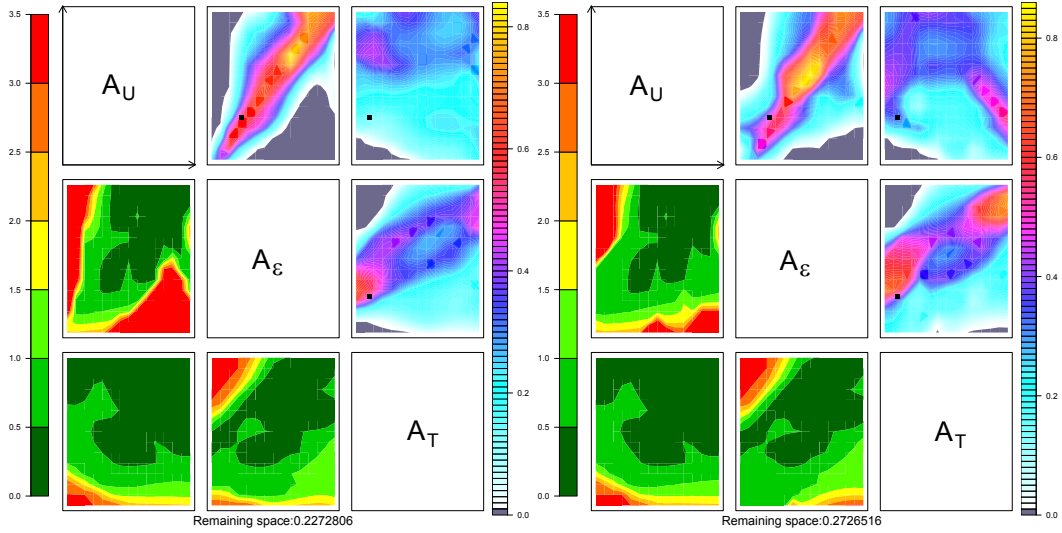


Figure 5. The left panel corresponds to the result of Exp1-3 and the right panel to Exp2-2. The upper right triangle contains 3 subfigures showing 2D sub-matrix. Each sub-matrix is a restriction to 2 parameters, the name of which are given in the diagonal of the main figure, and presents in colors the fraction of points with implausibility smaller than the threshold (here a value of 3). This fraction is obtained by fixing the two parameters at values of the x-axis and y-axis of the plotted location and searching the other dimensions (here the third dimension as we have only three parameters) of the parameter space. This allows to visualize in 2-D the full NROY which is 3-D here but can be n-D if n parameters are selected. The lower left triangle (with also 3 subfigures) presents the minimum value of Implausibility. These plots are orientated the same way as those on the upper triangle, for easier visual comparison. The black dots correspond to the default values used in the model.

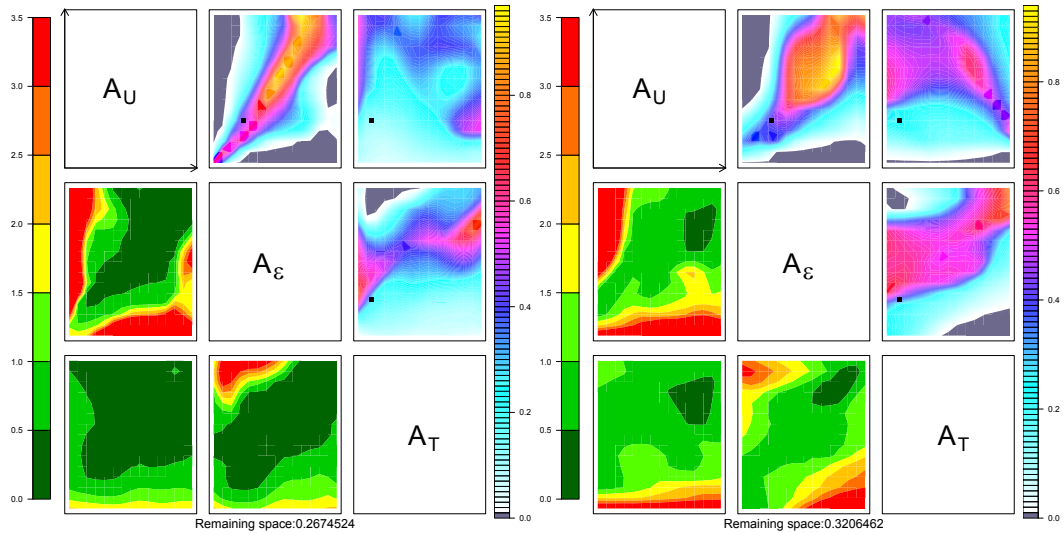


Figure 6. Same as Fig. 5 but for the sensitivity to the number of SCM runs (Experiment 4, left panel) and to the tolerance error (Experiment 5, right panel).

825 5 Conclusion

826 In this paper, we make a proposal to accelerate weather and climate model devel-
 827 opment. Our proposal tackles model development and calibration jointly. For that pur-
 828 pose, we have developed a tool that formalizes a process-based calibration, the *High-Tune*
 829 *Explorer* made available to the other modeling groups. It extensively exploits the SCM/LES
 830 comparison on a multicases, multi-metrics basis and benefits from machine learning tech-
 831 niques. In contrast with other recent proposals to use machine learning techniques in cli-
 832 mate modeling, we keep parameterizations as key ingredients of these models because
 833 they summarize our current understanding of the main physical processes This choice
 834 is motivated in particular by the confidence needed when extrapolating the model re-
 835 sults to a future climate.

836 The tool allows us to define the sub-domain of the parameter values for which SCM
 837 matches LES on selected metrics for a series of cases within a given uncertainty. The ex-
 838 ploration of the free-parameter space is facilitated using Gaussian process emulators. These

839 emulators, once trained on a limited number of real simulations, predict the SCM with
840 uncertainty in a much shorter time than required to run the SCM. History matching us-
841 ing the emulator is performed iteratively to progressively shrink the space of acceptable
842 parameter values. This iterative approach contrasts with the more traditional tuning strat-
843 egy based on optimization, which i) seeks an individual “best” value where the SCM min-
844 imizes a cost function computed for given metrics, ii) is strongly dependent on the weights
845 given to the metrics and iii) is highly sensitive to the choice of metrics. By pursuing a
846 strategy for discarding parameter values, we are left with a free parameter domain that
847 is (i) consistent with the metrics we have chosen, (ii) can be further reduced by intro-
848 ducing new metrics or altering our tolerance to model error, and (iii) does not claim a
849 single best simulation which may be over-fitted to one or more metrics, needlessly bi-
850 asing the simulation and potentially leading to less physical behavior, as the model is
851 projected into different regimes, than other choices in our not-ruled-out-yet space. Our
852 tool formalizes the consideration of the different sources of uncertainties associated to
853 the reference, the statistical tool and the model. For the latter, we take a “tolerance to
854 error” approach, allowing the question of whether a parameterization can match our ref-
855 erence as well as we think it ought to (based on any physical limitations we believe should
856 be there), and enabling us to revisit those expectations and to understand the model’s
857 limitations throughout the process.

858 In the present study, we present applications of the *High-Tune Explorer* to the SCM/LES
859 framework, focused on the representation of the atmospheric boundary layer. We have il-
860 lustrated how this tool allows us to objectively verify choices that have been made by
861 model developers for the free-parameter values. Experimenting with the combination of
862 the metrics with this tool allows us to clarify the importance of a given metric, the num-
863 ber or combination of metrics that should be used, and the possible redundancy between
864 metrics all in an efficient way that was not possible without it. The tool also enables us
865 to include new metrics at a new iteration so that we can pursue the calibration exercise,
866 even though one realizes an important deficiency of the model is not addressed by the
867 previously selected metrics. Our framework allows a progressive addition of metrics, cases
868 or a gradual reduction of the tolerance to error and is therefore very flexible.

869 Although this new framework is tested here for the improvement of boundary-layer
870 processes (turbulent transport in Part I and cloud representation in Part II) by running
871 the full atmospheric physics on one model column considering well established test cases

872 for which LES are particularly relevant, it has much broader application. It can be used
873 for instance to calibrate elementary pieces of parameterization (e.g., entrainment formu-
874 lation) without time integration. This methodology can be easily expanded to other pa-
875 rameterizations as well. The key ingredient for doing this is a reliable reference with doc-
876 umented uncertainty. This reference could come either from a detailed modeling of the
877 process, as done here with LES, or from observations as long as the other sources of dis-
878 crepancy as the uncertainty coming from the case definition are documented. Propos-
879 ing new relevant metrics and estimation of associated uncertainties will become valuable
880 now that we know how to include them in the model improvement process. An effort is
881 currently done in that direction in parallel to the work presented here, consisting in pro-
882 viding reference radiative transfer computations on the classical cloud test cases currently
883 used for parameterization development or (here) tuning. The development of the param-
884 eterization of boundary layer and clouds based on SCM/LES comparisons was indeed
885 focused so far on the representation of atmospheric transport and macrophysics of clouds,
886 but the radiative transfer computations run in LES models were often not more reliable
887 than those used in GCM. By developing fast and accurate radiative tools that accounts
888 for the full 3D radiative transfer in LES cloud scheme, as proposed by Villefranque et al.
889 (2019), we can compute many types of radiative metrics, from monochromatic, local, and
890 directional observable to integrated energetic quantities. The use of such radiative met-
891 rics will allow us to tackle calibration of radiative parameterizations but also to better
892 link the calibration realized at the level of the parameterizations itself with the one re-
893 alized for the final full 3D model calibration, which mainly targets the radiative forcing
894 of the atmospheric general circulation.

895 To sum-up, the application of the *High-Tune Explorer* on SCM/LES comparisons
896 allows us: (i) to quantify the parametric uncertainty at process level, (ii) to identify pa-
897 rameters which limit model performance, whatever their value, and should be replaced
898 by a more physical parameterization, and (ii) to reduce the domain of acceptable val-
899 ues of free parameters used in the final tuning of the global model.

900 We show indeed in Part II how the tool applied first to SCM/LES comparisons,
901 on a multicase basis, can be used to reduce the range of acceptable values for the cal-
902 ibration of the complete 3D model configuration and considerably accelerate the resource
903 and time consumption for this step of model development. The final 3D tuning becomes

904 a part of the history matching process, by adding new metrics or constraints using the
 905 exact same codes.

906 We believe that this tool is a breakthrough for model development as it allows us
 907 to place the importance of the physical understanding of the processes at the heart of
 908 model development, based on an extensive use of the SCM/LES comparison, whilst har-
 909 nassing important techniques in machine learning and uncertainty quantification. We
 910 advocate that the approach presented here leads to a well-defined strategy for calibra-
 911 tion of the full model that may change the way we do climate modeling and result in a
 912 significant acceleration in model improvement.

913 **Appendix A The different Large-Eddy Simulations**

914 In total, eight different simulations have been run with Meso-NH (Lac et al., 2018),
 915 varying the resolution, domain size, turbulence formulation, intensity of the white noise
 916 introduced at the first level and initial time to trigger turbulence, activation of subgrid
 917 condensation and changes in the microphysics scheme for the cloudy cases. The Table A1
 918 lists the different simulations of the Ayotte case used in Sect. 4 to estimate the uncer-
 919 tainty associated to the reference LES and the Table A2 lists the different simulations
 920 of the ARMCU case used in Sect. 3 to estimate the uncertainty associated to the ref-
 921 erence LES. The reference LES is highlighted in bold.

922 **Acknowledgments**

923 This work received funding from grant HIGH-TUNE ANR-16-CE01-0010. It was sup-
 924 ported by the DEPHY2 project, funded by the French national program LEFE/INSU
 925 and the GDR-DEPHY.B beyond the presentation of a new approach that we think could
 926 constiute a break through in climate model improvement, we intend to provide a tool
 927 for the climate community. All the programs, scripts and reference LES used will be made
 928 available together with the paper.

929 **References**

930 Ahmat Younous, A.-L., Roehrig, R., Beau, I., & Douville, H. (2018). Single-column
 931 modeling of convection during the cindy2011/dynamo field campaign with
 932 the cnrm climate model version 6. *Journal of Advances in Modeling Earth*
 933 *Systems*, 10, 578–602.

Table A1. List of the different LES runs of the Ayotte case used to determine the uncertainty around the reference

Name	Resolution	White noise	Turbulence	Diffusion
Name	Dx, Dz	Standard deviation (K)	length-scale	Timescale
Reference	50 m,nested <25 m	0.01 K	Deardorff length scale	1800 s
WhiteNoise	”	0.1 K	”	”
WhiteNoiseLL	”	0.5 K	”	”
Turb	”	”	size of the grid	”
Difshort	”	”	”	300 s
Diflong	”	”	”	7200 s
Dx	25 m, ”	”	”	”
Dz	”, nested <12.5 m	”	”	”

- 934 Andrianakis, I., McCreesh, N., Vernon, I., McKinley, T. J., Oakley, J. E., Nsub-
935 uga, R. N., ... White, R. G. (2017). Efficient history matching of a high
936 dimensional individual-based hiv transmission model. *SIAM/ASA Journal on*
937 *Uncertainty Quantification*, 5(1), 694–719.
- 938 Ayotte, K. W., Sullivan, P. P., Andren, A., Doney, S. C., Holtslag, A. A., Large,
939 W. G., ... Wyngaard, J. C. (1996). An evaluation of neutral and convective
940 planetary boundary-layer parameterizations relative to large eddy simulations.
941 *Boundary-layer Meteorol.*, 79, 131–175.
- 942 Bony, S., Stevens, B., Frierson, D. M. W., Jakob, C., Kageyama, M., Pincus, R.,
943 ... Webb, M. J. (2015, April). Clouds, cirulation and climate sensitiv-
944 ity. *Nature Geoscience*, 8(20), L20806. (WOS:000233104900005) doi:
945 10.1038/NGEO2398
- 946 Bougeault, P., & Lacarrere, P. (1989). Parameterization of orography induced turbu-
947 lence in a mesobeta-scale model. *Mon. Wea. Rev.*, 117, 1872–1890.
- 948 Brenowitz, N. D., & Bretherton, C. S. (2018, June). Prognostic validation of a
949 neural network unified physics parameterization. *Geophysical Research Letters*,
950 45(12), 6289–6298. (WOS:000438499100052) doi: 10.1029/2018GL078510

Table A2. List of the different LES runs of the ARMCU case used to determine the uncertainty around the reference; the names indicated in the left column are those used in the legend of Figure 2

Name	Horizontal Resolution	Vertical Resolution	Domain side	Subgrid Condensation	Microphysics	Turbulence mixing length
12Dx25z25	25 m	25 m	12.8 km	No	Warm (ICE3)	Deardorff
6Dx25z25	”	”	6.4 km	”	”	”
6Dx40z25	40 m	25 m	6.4 km	”	”	”
6Dx40z40	40 m	40 m	6.4 km	”	”	”
6Dx25zvar	25 m	stretched grid	6.4 km	”	”	”
6Dx100z40	100 m	40 m	6.4 km	”	”	”
25Dx100z40	100 m	40 m	25.6 km	”	”	”
51Dx100z40	100 m	40 m	51.2 km	”	”	”
6DelDx25z25	25 m	25 m	6.4 km	”	”	$(Dx * Dy * Dz)^{1/3}$
6SbgDx25z25	25 m	25 m	6.4 km	Yes	”	Deardorff
6NprDx25z25	25 m	25 m	6.4 km	No	Only saturation adjustment	”

- 951 Brient, F., Couvreux, F., Villefranque, N., Rio, C., & Honnert, R. (2019). Object-
 952 oriented identification of coherent structures in large eddy simulations: Im-
 953 portance of downdrafts in stratocumulus. *Geophysical Research Letters*, *46*,
 954 2854–2864.
- 955 Brown, A. R. (1999, January). The sensitivity of large-eddy simulations of shallow
 956 cumulus convection to resolution and subgrid model. *Quarterly Journal of the*
 957 *Royal Meteorological Society*, *125*(554), 469–482. (WOS:000079350100004) doi:
 958 10.1002/qj.49712555405
- 959 Brown, A. R., Cederwall, R. T., Chlond, A., Duynkerke, P. G., Golaz, M., J.
 960 C. Khairoutdinov, Lewellen, D. C., ... Stevens, B. (2002). Large-eddy simu-
 961 lation of the diurnal cycle of shallow cumulus convection over land. *Q. J. R.*
 962 *Meteorol. Soc.*, *128*, 1075–1093.
- 963 Browning, K., Betts, A., Jonas, P., Kershaw, R., Manton, M., Mason, P.,
 964 ... Simpson, J. (1993, March). The GEWEX Cloud System Study
 965 (GCSS). *Bulletin of the American Meteorological Society*, *74*(3), 387–399.
 966 (WOS:A1993KU53500004)
- 967 Brynjarsdóttir, J., & O’Hagan, A. (2014). Learning about physical parameters: The
 968 importance of model discrepancy. *Inverse Problems*, *30*(11), 114007.
- 969 Caldwell, P., & Bretherton, C. S. (2009, January). Response of a Subtropi-
 970 cal Stratocumulus-Capped Mixed Layer to Climate and Aerosol Changes.
 971 *Journal of Climate*, *22*(1), 20–38. (WOS:000262329100002) doi: 10.1175/
 972 2008JCLI1967.1
- 973 Carpenter, B., & Coauthors. (2017, May). Stan: A probabilistic programming lan-
 974 guage. *Journal of Statistical Software*, *76*(1), 00–00. doi: 10.18637/jss.v076
 975 .i01
- 976 Chinita, M. J., Matheou, G., & Teixeira, J. (2018). A joint probability density
 977 based decomposition of turbulence in the atmospheric boundary layer. *Monthly*
 978 *Weather Review*, *146*, 503–523.
- 979 Couvreux, F., Guichard, F., Redelsperger, J. L., Kiemle, C., Masson, V., Lafore,
 980 J. P., & Flamant, C. (2005, October). Water-vapour variability within a
 981 convective boundary-layer assessed by large-eddy simulations and IHOP_2002
 982 observations. *Quarterly Journal of the Royal Meteorological Society*, *131*(611),
 983 2665–2693. (WOS:000233475900005) doi: 10.1256/qj.04.167

- 984 Couvreur, F., Hourdin, F., & Rio, C. (2010, March). Resolved Versus Parametrized
 985 Boundary-Layer Plumes. Part I: A Parametrization-Oriented Conditional
 986 Sampling in Large-Eddy Simulations. *Boundary-Layer Meteorology*, *134*(3),
 987 441–458. (WOS:000274013600004) doi: 10.1007/s10546-009-9456-5
- 988 Craig, P. S., Goldstein, M., Seheult, A., & Smith, J. (1996). Bayes linear strategies
 989 for matching hydrocarbon reservoir history. *Bayesian statistics*, *5*, 69–95.
- 990 Cuxart, J., Bougeault, P., & Redelsperger, J.-L. (2000). A turbulence scheme allow-
 991 ing for mesoscale and large-eddy simulations. *Q. J. R. Meteorol. Soc.*, *126*, 1–
 992 30.
- 993 Duynkerke, P. G., de Roode, S. R., van Zanten, M. C., Calvo, J., Cuxart, J., &
 994 Cheinet, S. (2004). Observations and numerical simulations of the diurnal
 995 cycle of the eurocs stratocumulus case. *Quarterly Journal of the Royal Meteo-*
 996 *rological Society*, *130*, 3269–3296.
- 997 Flato, J., G. and Marotzke, Abiodun, B., Braconnot, P., Chou, S., Collins, W., Cox,
 998 P., ... Rummukaine, M. (2013, August). Evaluation of climate models. *Cli-*
 999 *mate Change 2013: The Physical Science Basis. Contribution of Working*
 1000 *Group I to the Fifth Assessment Report of the Intergovernmental Panel on*
 1001 *Climate Change*.
- 1002 Gelman, A. (2006). Prior distributions for variance parameters in hierarchical mod-
 1003 els. *Bayesian Analysis*, *1*, 515–534.
- 1004 Gentine, P., Pritchard, M., Rasp, S., Reinaudi, G., & Yacalis, G. (2018, May). Could
 1005 machine learning break the convection parameterization deadlock? *Geophysical*
 1006 *Research Letters*, *45*, 5742–5751. doi: 10.1029/2018GL078202
- 1007 Gettelman, A., Truesdale, J., Bacmeister, J., Caldwell, P., Neale, R., & Bogenschutz,
 1008 P. (2019, May). The single column atmosphere model version 6 (scam6): Not a
 1009 scam but a tool for model evaluation and development. *Journal of Advances in*
 1010 *modeling earth systems*, *11*, 1381–1401. doi: 10.1029/2018MS001578
- 1011 Golaz, J.-C., Horowitz, L. W., & Levy, H. (2013, May). Cloud tuning in a cou-
 1012 pled climate model: Impact on 20th century warming. *Geophysical Research*
 1013 *Letters*, *40*(10), 2246–2251. (WOS:000328840200064) doi: 10.1002/grl.50232
- 1014 Golaz, J. C., Larson, V. E., & Cotton, W. R. (2002, December). A PDF-based
 1015 model for boundary layer clouds. Part II: Model results. *Journal of the Atmo-*
 1016 *spheric Sciences*, *59*(24), 3552–3571. (WOS:000179629800007) doi: 10.1175/

- 1017 1520-0469(2002)059(3552:APBMFB)2.0.CO;2
- 1018 Grabowski, W. W. (2016, June). Towards global large-eddy simulation: super pa-
 1019 rameterization revisited. *Journal of the Meteorological Society of Japan*, *94*(4),
 1020 L20806. doi: 10.2151/jmsj.2016-017
- 1021 Gueremy, J. F. (2011, August). A continuous buoyancy based convection scheme:
 1022 one- and three-dimensional validation. *Tellus Series a-Dynamic Meteorology*
 1023 *and Oceanography*, *63*(4), 687–706. (WOS:000292864500004) doi: 10.1111/j
 1024 .1600-0870.2011.00521.x
- 1025 Guichard, F., & Couvreur, F. (2017). A short review of numerical cloud-
 1026 resolving models. *Tellus Dyn. Meteorol. Oceanogr.*, *69*, 1945–1960. doi:
 1027 10.1080/16000870.2017.1373578
- 1028 Heus, T., & Jonker, H. J. J. (2008, March). Subsiding shells around shallow
 1029 cumulus clouds. *Journal of the Atmospheric Sciences*, *65*(3), 1003–1018.
 1030 (WOS:000254356600016) doi: 10.1175/2007JAS2322.1
- 1031 Heus, T., Pols, C. F. J., Jonker, H. J. J., Van den Akker, H. E. A., & Lenschow,
 1032 D. H. (2009, January). Observational validation of the compensating mass
 1033 flux through the shell around cumulus clouds. *Quarterly Journal of the Royal*
 1034 *Meteorological Society*, *135*(638), 101–112. (WOS:000265374900008) doi:
 1035 10.1002/qj.358
- 1036 Holtslag, A. A. M., Svensson, G., Baas, P., Basu, S., Beare, B., Beljaars, A. C. M.,
 1037 ... Van de Wiel, B. J. H. (2013, November). STABLE ATMOSPHERIC
 1038 BOUNDARY LAYERS AND DIURNAL CYCLES Challenges for Weather
 1039 and Climate Models. *Bulletin of the American Meteorological Society*, *94*(11),
 1040 1691–1706. (WOS:000327926700007) doi: 10.1175/BAMS-D-11-00187.1
- 1041 Hourdin, F., Couvreur, F., & Menut, L. (2002, March). Parameterization
 1042 of the dry convective boundary layer based on a mass flux representa-
 1043 tion of thermals. *Journal of the Atmospheric Sciences*, *59*(6), 1105–
 1044 1123. (WOS:000174019900006) doi: 10.1175/1520-0469(2002)059(1105:
 1045 POTDCB)2.0.CO;2
- 1046 Hourdin, F., Grandpeix, J.-Y., Rio, C., Bony, S., Jam, A., Cheruy, F., ... Roehrig,
 1047 R. (2013, May). LMDZ5b: the atmospheric component of the IPSL cli-
 1048 mate model with revisited parameterizations for clouds and convection.
 1049 *Climate Dynamics*, *40*(9-10), 2193–2222. (WOS:000318278700005) doi:

- 1050 10.1007/s00382-012-1343-y
- 1051 Hourdin, F., Mauritsen, T., Gettelman, A., Golaz, J.-C., Balaji, V., Duan, Q., ...
 1052 Williamson, D. (2017, March). The Art and Science of Climate Model Tuning.
 1053 *Bull. Am. Meteorol. Soc.*, *98*, 589-602. doi: 10.1175/BAMS-D-15-00135.1
- 1054 Hourdin, F., Rio, C., Grandpeix, J.-Y., Madeleine, J.-B., Cheruy, F., Rochetin,
 1055 N., ... Ghattas, J. (2020, June). LMDZ6A: the atmospheric component
 1056 of the ipsl climate model with improved and better tuned physics. *Journal*
 1057 *of Advances in modeling earth systems, accepted for publication, ??-??* doi:
 1058 10.1029/2019MS001892
- 1059 Jakob, C. (2010, July). ACCELERATING PROGRESS IN GLOBAL ATMO-
 1060 SPHERIC MODEL DEVELOPMENT THROUGH IMPROVED PARAM-
 1061 ETERIZATIONS Challenges, Opportunities, and Strategies. *Bulletin of the*
 1062 *American Meteorological Society*, *91*(7), 869+. (WOS:000280758700003) doi:
 1063 10.1175/2009BAMS2898.1
- 1064 Jam, A., Hourdin, F., Rio, C., & Couvreux, F. (2013, June). Resolved Versus
 1065 Parametrized Boundary-Layer Plumes. Part III: Derivation of a Statistical
 1066 Scheme for Cumulus Clouds. *Boundary-Layer Meteorology*, *147*(3), 421-441.
 1067 (WOS:000319475000004) doi: 10.1007/s10546-012-9789-3
- 1068 Jiang, J. H., Su, H., Zhai, C., Perun, V., Del Genio, A., Nazarenko, L. S., ... L,
 1069 S. G. (2012, July). Evaluation of cloud and water vapor simulations in CMIP5
 1070 climate models using nasa "a-train" satellite observations. *Journal of Geophysi-*
 1071 *cal Research*, *117*, 1-24. doi: 10.1029/2011JD017237
- 1072 Kennedy, M. C., & O'Hagan, A. (2001, aug). Bayesian calibration of computer mod-
 1073 els. *Journal of the Royal Statistical Society: Series B (Statistical Methodology)*,
 1074 *63*(3), 425-464. Retrieved from [http://doi.wiley.com/10.1111/1467-9868](http://doi.wiley.com/10.1111/1467-9868.00294)
 1075 [.00294](http://doi.wiley.com/10.1111/1467-9868.00294) doi: 10.1111/1467-9868.00294
- 1076 Khairoutdinov, M., Randall, D., & DeMott, C. (2005, July). Simulations of the
 1077 atmospheric general circulation using a cloud-resolving model as a superpa-
 1078 rameterization of physical processes. *Journal of the Atmospheric Sciences*,
 1079 *62*(7), 2136-2154. (WOS:000230962800006) doi: 10.1175/JAS3453.1
- 1080 Klein, S. A., Hall, A., R., N. J., & Robert, P. (2017, October). Low-cloud feedbacks
 1081 from cloud-controlling factors: a review. *Survey of Geophysics*, *38*(10), 1307-
 1082 1329. doi: 10.1007/s10712-017-9433-3

- 1083 Krasnopolsky, V. M., Fox-Rabinovitz, M. S., & Belochitski, A. A. (2013, March).
 1084 Using ensemble of neural networks to learn stochastic convection parameteriza-
 1085 tions for climate and numerical weather prediction models from data simulated
 1086 by a cloud resolving model. *Advances in Artificial Neural Systems*, 203(3), 13.
 1087 doi: 10.1155/2013/485913
- 1088 Lac, C., Chaboureau, J.-P., Masson, V., Pinty, J.-P., Tulet, P., Escobar, J., ...
 1089 Wautelet, P. (2018, January). Overview of the Meso-NH model version 5.4 and
 1090 its applications. *Geosci. Model Dev. Discuss.*, 2018, 1–66. Retrieved 2018-03-
 1091 26, from <https://www.geosci-model-dev-discuss.net/gmd-2017-297/> doi:
 1092 10.5194/gmd-2017-297
- 1093 Matheou, G., Chung, D., Nuijens, L., Stevens, B., & Teixeira, J. (2011, Septem-
 1094 ber). On the Fidelity of Large-Eddy Simulation of Shallow Precipitat-
 1095 ing Cumulus Convection. *Monthly Weather Review*, 139(9), 2918–2939.
 1096 (WOS:000294932100014) doi: 10.1175/2011MWR3599.1
- 1097 Mauritsen, T., Stevens, B., Roeckner, E., Crueger, T., Esch, M., Giorgetta, M., ...
 1098 Tomassini, L. (2012, August). Tuning the climate of a global model. *Journal*
 1099 *of Advances in Modeling Earth Systems*, 4, M00A01. (WOS:000307467200001)
 1100 doi: 10.1029/2012MS000154
- 1101 McNeall, D., Williams, J., Betts, R., Booth, B., Challenor, P., Good, P., & Wilt-
 1102 shire, A. (2019). Correcting a bias in a climate model with an augmented
 1103 emulator. *Geoscientific Model Development Discussions*, 2019, 1–37. Retrieved
 1104 from <https://www.geosci-model-dev-discuss.net/gmd-2019-171/> doi:
 1105 10.5194/gmd-2019-171
- 1106 Nam, C., Bony, S., Dufresne, J.-L., & Chepfer, H. (2012, November). The ‘too few,
 1107 too bright’ tropical low-cloud problem in CMIP5 models. *Geophysical Research*
 1108 *Letters*, 39, L21801. (WOS:000310690600003) doi: 10.1029/2012GL053421
- 1109 Neggers, R. A. J. (2009, June). A Dual Mass Flux Framework for Boundary Layer
 1110 Convection. Part II: Clouds. *Journal of the Atmospheric Sciences*, 66(6),
 1111 1489–1506. (WOS:000267263300002) doi: 10.1175/2008JAS2636.1
- 1112 Neggers, R. A. J. (2015, December). Attributing the behavior of low-level clouds in
 1113 large-scale models to subgrid-scale parameterizations. *Journal of Advances in*
 1114 *modeling earth systems*, 7(4), 2029–2043. doi: 10.1002/2015MS000503
- 1115 Neggers, R. A. J., Ackerman, A. S., Angevine, W. M., Bazile, E., Beau, I., Blossey,

- 1116 P. N., . . . Heus, T. (2017, October). Single-column model simulations of
 1117 subtropical marine boundary-layer cloud transitions under weakening inver-
 1118 sions. *Journal of Advances in modeling earth systems*, *9*(6), 2385–2412. doi:
 1119 10.1002/2017MS001064
- 1120 Neggers, R. A. J., Duynkerke, P. G., & Rodts, S. M. A. (2003, July). Shallow cu-
 1121 mulus convection: A validation of large-eddy simulation against aircraft and
 1122 Landsat observations. *Quarterly Journal of the Royal Meteorological Society*,
 1123 *129*(593), 2671–2696. (WOS:000185187600011) doi: 10.1256/qj.02.93
- 1124 Neggers, R. A. J., J, J. H. J., & Siebesma, P. (2003). Statistics of cumulus cloud
 1125 populations in large-eddy simulations. *J. Atmos. Sci.*, *60*, 1060–1074.
- 1126 Neggers, R. A. J., Siebesma, A. P., & Heus, T. (2012, September). Continu-
 1127 ous single-column model evaluation at a permanent meteorological super-
 1128 site. *Bulletin of the American Meteorological Society*, *93*(9), 1389–1400.
 1129 (WOS:000309056400006) doi: 10.1175/BAMS-D-11-00162.1
- 1130 Neggers, R. A. J., Siebesma, A. P., Lenderink, G., & Holtslag, A. A. M. (2004,
 1131 November). An evaluation of mass flux closures for diurnal cycles
 1132 of shallow cumulus. *Monthly Weather Review*, *132*(11), 2525–2538.
 1133 (WOS:000225098900001) doi: 10.1175/MWR2776.1
- 1134 Neggers, R. A. J., Siebesma, P., & J, J. H. J. (2002). A multiparcel model for shal-
 1135 low cumulus convection. *J. Atmos. Sci.*, *59*, 1655–1668.
- 1136 Nuijens, L., Medeiros, B., Sandu, I., & Ahlgrim, M. (2015, December). Observed
 1137 and modeled patterns of covariability between low-level cloudiness and the
 1138 structure of the trade-wind layer. *Journal of Advances in Modeling Earth Sys-*
 1139 *tems*, *7*(4), 1741–1764. (WOS:000368739800013) doi: 10.1002/2015MS000483
- 1140 Oakley, J. E., & O’Hagan, A. (2004, December). Probabilistic sensitivity analysis
 1141 of complex models: a bayesian approach. *Royal Statistical Society*, *66*(3), 751–
 1142 769.
- 1143 Parishani, H., Pritchard, M., Bretherton, C., Wyant, M., & Khairoutdinov, M.
 1144 (2017, May). Toward low-cloud-permitting cloud superparameterization with
 1145 explicit boundary layer turbulence. *Journal of Advances in modeling earth*
 1146 *systems*, *9*, 1542–1571. doi: 10.1002/2018MS001409
- 1147 Pergaud, J., Masson, V., Malardel, S., & Couvreux, F. (2009, July). A Param-
 1148 eterization of Dry Thermals and Shallow Cumuli for Mesoscale Numeri-

- 1149 cal Weather Prediction. *Boundary-Layer Meteorology*, 132(1), 83–106.
 1150 (WOS:000267029600006) doi: 10.1007/s10546-009-9388-0
- 1151 Piriou, J.-M., Redelsperger, J.-L., Geleyn, J.-F., Lafore, J.-P., & Guichard, F. (2007,
 1152 November). An approach for convective parameterization with memory: Sep-
 1153 arating microphysics and transport in grid-scale equations. *Journal of the At-*
 1154 *mospheric Sciences*, 64(11), 4127–4139. (WOS:000251283000025) doi: 10
 1155 .1175/2007JAS2144.1
- 1156 Pressel, K. G., Mishra, S., Schneider, T., Kaul, C. M., & Tan, Z. (2017, June). Nu-
 1157 merics and subgrid-scale modeling in large eddy simulations of stratocumulus
 1158 clouds. *Journal of Advances in Modeling Earth Systems*, 9(2), 1342–1365. doi:
 1159 10.1002/2016MS000778
- 1160 Pukelsheim, F. (1994, February). The three sigma rule. *The American Statistician*,
 1161 48, 88–91.
- 1162 Randall, D., Khairoutdinov, M., Arakawa, A., & Grabowski, W. (2003, November).
 1163 Breaking the cloud parameterization deadlock. *Bulletin of the American Mete-*
 1164 *orological Society*, 84(11), 1547–1564. (WOS:000187163900019) doi: 10.1175/
 1165 BAMS-84-11-1547
- 1166 Randall, D., Xu, K., Somerville, R., & Iacobellis, S. (1996, August). Single-column
 1167 models and cloud ensemble models as links between observations and climate
 1168 models. *Journal of Climate*, 9(8), 1683–1697. (WOS:A1996VG92100002) doi:
 1169 10.1175/1520-0442(1996)009<1683:SCMACE>2.0.CO;2
- 1170 Richter, I. (2015, February). Climate model biases in the eastern tropical oceans:
 1171 Causes, impacts and ways forward. *Wiley Interdisciplinary Reviews:Climate*
 1172 *Change*, 6(3), 345–358.
- 1173 Rio, C., Del Genio, A. D., & F, H. (2019). Ongoing breakthroughs in convective pa-
 1174 rameterization. *Current Climate Change Reports*, 5, 95–111.
- 1175 Rio, C., & Hourdin, F. (2008, February). A thermal plume model for the convective
 1176 boundary layer: Representation of cumulus clouds. *Journal of the Atmospheric*
 1177 *Sciences*, 65(2), 407–425. (WOS:000253406600007) doi: 10.1175/2007JAS2256
 1178 .1
- 1179 Rio, C., Hourdin, F., Couvreux, F., & Jam, A. (2010, June). Resolved Versus
 1180 Parametrized Boundary-Layer Plumes. Part II: Continuous Formulations of
 1181 Mixing Rates for Mass-Flux Schemes. *Boundary-Layer Meteorology*, 135(3),

- 1182 469–483. (WOS:000277635800007) doi: 10.1007/s10546-010-9478-z
- 1183 Rochetin, N., Couvreur, F., Grandpeix, J.-Y., & Rio, C. (2014, February). Deep
 1184 Convection Triggering by Boundary Layer Thermals. Part I: LES Analysis
 1185 and Stochastic Triggering Formulation. *Journal of the Atmospheric Sciences*,
 1186 *71*(2), 496–514. (WOS:000335491400003) doi: 10.1175/JAS-D-12-0336.1
- 1187 Roehrig, R., Beau, I., Saint-Martin, D., Alias, A., Colin, J., Decharme, B., ...
 1188 S n si, S. (2020, June). The CNRM global atmosphere model ARPEGE-
 1189 Climat 6.3: description and evaluation. *Journal of Advances in modeling earth*
 1190 *systems, accepted for publication, ??-??* doi: 10.1029/2020MS002075
- 1191 Saltelli, A. J. (2002, December). Making best use of model evaluations to compute
 1192 sensitivity indices. *Computer Physics Communications*, *145*(2), 280–297.
- 1193 Salter, J. M., Williamson, D. B., Scinocca, J., & Kharin, V. (2019, October).
 1194 Uncertainty quantification for computer models with spatial output using
 1195 calibration-optimal bases. *Journal of the American statistical association*,
 1196 *114*(528), 1800–1814. doi: 10.1080/01621459.2018.1514306
- 1197 Sandu, I., Beljaars, A., Bechtold, P., Mauritsen, T., & Balsamo, G. (2013). Why
 1198 is it so difficult to represent stably stratified conditions in numerical weather
 1199 prediction (NWP) models? *Journal of Advances in Modeling Earth Systems*,
 1200 *5*(2), 117–133. Retrieved from <http://dx.doi.org/10.1002/jame.20013> doi:
 1201 10.1002/jame.20013
- 1202 Satoh, M., Matsuno, T., Tomita, H., Miura, H., Nasuno, T., & Iga, S. (2008,
 1203 March). Nonhydrostatic icosahedral atmospheric model (NICAM) for global
 1204 cloud resolving simulations. *Journal of Computational Physics*, *227*(7), 3486–
 1205 3514. (WOS:000255005900005) doi: 10.1016/j.jcp.2007.02.006
- 1206 Satoh, M., Stevens, B., Judt, F., Khairoutdinov, M., Lin, S.-J., Putman, W., & P.,
 1207 D. (2019, September). Global cloud-resolving models. *Current Climate Change*
 1208 *Reports*, *5*(3), 172–184. doi: 10.1007/s40641-019-00131-0
- 1209 Schneider, T., Lan, T., Stuart, A., & Teixeira, J. (2017, December). Earth sys-
 1210 tem modeling 2.0: A blueprint for models that learn from observations and
 1211 targeted high-resolution simulations. *Geophysical Research Letters*, *44*, 12396–
 1212 12417. doi: 10.1002/2017GL076101
- 1213 Sexton, D. M., Murphy, J. M., Collins, M., & Webb, M. J. (2011, October). Multi-
 1214 variate probabilistic projections using imperfect climate models part i: outline

- 1215 of methodology. *Climate Dynamics*, *38*(1), 2513–2542.
- 1216 Siebesma, A. P., Bretherton, C. S., Brown, A., Chlond, A., Cuxart, J., Duynkerke,
1217 P. G., . . . Stevens, D. E. (2003). A large eddy simulation intercomparison
1218 study of shallow cumulus convection. *J. Atmos. Sci.*, *60*, 1201–1219.
- 1219 Siebesma, A. P., & Cuijpers, J. W. M. (1995). Evaluation of parametric assumptions
1220 for shallow cumulus convection. *J. Atmos. Sci.*, *52*, 650–666.
- 1221 Siebesma, A. P., Soares, P. M. M., & Teixeira, J. (2007, April). A combined eddy-
1222 diffusivity mass-flux approach for the convective boundary layer. *Journal of*
1223 *the Atmospheric Sciences*, *64*(4), 1230–1248. (WOS:000245742600011) doi:
1224 10.1175/JAS3888.1
- 1225 Soares, P. M. M., Miranda, P. M. A., Siebesma, A. P., & Teixeira, J. (2004). An
1226 eddy-diffusivity/mass-flux parameterization for dry and shallow cumulus con-
1227 vection. *Q. J. R. Meteorol. Soc.*, *130*(604), 3365–3383.
- 1228 Stevens, B., Satoh, M., Auger, L., Bierchamp, J., Bretherton, C. S., Chen, X., . . .
1229 Chou, L. (2019). Dyamond: the dynamics of the atmospheric general circu-
1230 lation modeled on non-hydrostatic domains. *Progress in Earth and Planetary*
1231 *Science*, *6*, 1–17. doi: 10.1186/s40645-019-0304-z
- 1232 Sullivan, P. P., & Patton, E. G. (2011, October). The Effect of Mesh Resolution
1233 on Convective Boundary Layer Statistics and Structures Generated by Large-
1234 Eddy Simulation. *Journal of the Atmospheric Sciences*, *68*(10), 2395–2415.
1235 (WOS:000296034700014) doi: 10.1175/JAS-D-10-05010.1
- 1236 Suselj, K., Kurowski, M. J., & Teixeira, J. (2019, August). A unified eddy-
1237 diffusivity/mass-flux approach for modeling atmospheric convection. *Journal of*
1238 *the Atmospheric Sciences*, 2505–2537.
- 1239 Suselj, K., Teixeira, J., & Chung, D. (2013, July). A Unified Model for Moist Con-
1240 vective Boundary Layers Based on a Stochastic Eddy-Diffusivity/Mass-Flux
1241 Parameterization. *Journal of the Atmospheric Sciences*, *70*(7), 1929–1953.
1242 (WOS:000322125600005) doi: 10.1175/JAS-D-12-0106.1
- 1243 Tan, Z., Kaul, C. M., Pressel, G., K, Cohen, Y., Schneider, T., & Teixeira, J. (2018,
1244 March). An extended eddy-diffusivity mass-flux scheme for unified representa-
1245 tion of subgrid scale turbulence and convection. *Journal of Advances in Model-*
1246 *ing Earth Systems*, 770–800.
- 1247 vanZanten, M. C., Stevens, B., Nuijens, L., Siebesma, A. P., Ackerman, A. S., Bur-

- 1248 net, F., ... Wyszogrodzki, A. (2011). Controls on precipitation and cloudiness
 1249 in simulations of trade-wind cumulus as observed during RICO. *Journal of*
 1250 *Advances in Modeling Earth Systems*, 3, M06001. (WOS:000303198400003)
 1251 doi: 10.1029/2011MS000056
- 1252 Vernon, I., Goldstein, M., & Bower, R. (2010). Galaxy formation: a bayesian uncer-
 1253 tainty analysis. *Bayesian Analytics*, 5, 619–846.
- 1254 Villefranche, N., Fournier, R., Couvreur, F., Blanco, S., Eymet, V., Forest, V., &
 1255 Tregan, J. M. (2019). A path-tracing monte carlo library for 3-d radiative
 1256 transfer in highly resolved cloudy atmospheres. *Journal of Advances in Model-*
 1257 *ing Earth Systems*, 11, 2449–2473.
- 1258 Voldoire, A., Saint-Martin, D., Senesi, S., Decharme, B., Alias, A., Chevallier, M.,
 1259 ... Waldman, W., R (2019, August). Evaluation of CMIP6 deck experiments
 1260 with CNRM-CM6-1. *Journal of Advances in Modeling Earth Systems*, 11(7),
 1261 2177–2213. doi: 10.1029/2019MS001683
- 1262 Volodina, V. (2020). *Uncertainty quantification for complex computer models with*
 1263 *nonstationary output. bayesian optimal design for iterative refocussing* (Unpub-
 1264 lished doctoral dissertation). University of Exeter.
- 1265 Volodina, V., & Williamson, D. (2020, January). Diagnostics-driven nonstationary
 1266 emulators using kernel mixtures. *Journal of Uncertainty Quantification*, 8(1),
 1267 1–26.
- 1268 Wang, H., & Feingold, G. (2009, November). Modeling Mesoscale Cellular Struc-
 1269 tures and Drizzle in Marine Stratocumulus. Part I: Impact of Drizzle on the
 1270 Formation and Evolution of Open Cells. *Journal of the Atmospheric Sciences*,
 1271 66(11), 3237–3256. (WOS:000271689700001) doi: 10.1175/2009JAS3022.1
- 1272 Williamson, D. (2015, June). Exploratory ensemble designs for environmental
 1273 models using k-extended Latin Hypercubes. *Environmetrics*, 26(4), 268–283.
 1274 (WOS:000353380200003) doi: 10.1002/env.2335
- 1275 Williamson, D., Blaker, A. T., Hampton, C., & Salter, J. (2015, September). Iden-
 1276 tifying and removing structural biases in climate models with history match-
 1277 ing. *Climate Dynamics*, 45(5-6), 1299–1324. (WOS:000360507700010) doi:
 1278 10.1007/s00382-014-2378-z
- 1279 Williamson, D., Blaker, A. T., & Sinha, B. (2017, April). Tuning without over-
 1280 tuning: parametric uncertainty quantification for the NEMO ocean model.

- 1281 *Geoscientific Model Development*, 10(4), 1789–1816. (WOS:000400181200002)
1282 doi: 10.5194/gmd-10-1789-2017
- 1283 Williamson, D., Goldstein, M., Allison, L., Blaker, A., Challenor, P., Jackson, L.,
1284 & Yamazaki, K. (2013, October). History matching for exploring and
1285 reducing climate model parameter space using observations and a large
1286 perturbed physics ensemble. *Climate Dynamics*, 41(7-8), 1703–1729.
1287 (WOS:000324812200002) doi: 10.1007/s00382-013-1896-4
- 1288 Williamson, D., & Volodina, V. (2020). ExeterUQ mोगp an r interface to performing
1289 uq with mop emulator. *Documentation*. Retrieved from [https://bayesexeter](https://bayesexeter.github.io/ExeterUQ_MOGP/)
1290 [.github.io/ExeterUQ_MOGP/](https://bayesexeter.github.io/ExeterUQ_MOGP/)
- 1291 Wurps, H., Steinfeld, G., & Heinz, S. (2020, March). Grid-Resolution Requirements
1292 for Large-Eddy Simulations of the Atmospheric Boundary Layer. *Boundary-*
1293 *Layer Meteorology*, 175, 179–201. doi: 10.1007/s10546-020-00504-1
- 1294 Zhang, M., Somerville, R. C. J., & Xie, S. (2016, February). The scm concept and
1295 creation of arm forcing datasets. *Meteorological Monographs*, 57, 24.1–24.12.
1296 doi: 10.1175/AMSMONOGRAPHIS-D-15-0040.1
- 1297 Zhang, Y., Klein, S. A., Fan, J., Chandra, A. S., Kollias, P., Xie, S., & Tang, S.
1298 (2017, October). Large-Eddy Simulation of Shallow Cumulus over Land: A
1299 Composite Case Based on ARM Long-Term Observations at Its Southern
1300 Great Plains Site. *Journal of the Atmospheric Sciences*, 74(10), 3229–3251.
1301 doi: 10.1175/JAS-D-16-0317.1